

Probe of the shell crossing at $A=40$ via beta decay: Experiment and theory

E. K. Warburton and D. E. Alburger

Brookhaven National Laboratory, Upton, New York 11973

J. A. Becker

Lawrence Livermore National Laboratory, Livermore, California 94550

B. A. Brown

Cyclotron Laboratory, Michigan State University, East Lansing, Michigan 48824

S. Raman

Oak Ridge National Laboratory, Oak Ridge, Tennessee 37831

(Received 28 May 1986)

The β^- decays of ^{35}P , ^{37}S , ^{38}S , and ^{38}Cl were studied both experimentally and via shell-model calculations. The four decaying nuclei were formed by bombardment of 81% enriched ^{36}S by triton and deuteron beams. Gamma-ray spectroscopy was carried out with Ge detectors, either bare or surrounded by a Compton suppression NaI(Tl) shield. One new Gamow-Teller decay was observed in ^{35}P decay, and one new first-forbidden decay was observed in ^{38}S decay. Otherwise γ -ray measurements of E_γ and I_γ (and limits on I_γ for unobserved transitions) were improved significantly over previous results. Shell-model studies were undertaken in order to bring these beta decay results to bear on an understanding of the shell structure in the (sd) to (fp) transition region at $A=40$. An interaction was constructed in the $1d_{5/2}$, $1d_{3/2}$, $2s_{1/2}$, $1f_{7/2}$, $1f_{5/2}$, $1p_{3/2}$, $1p_{1/2}$ model space. This interaction started from the Wildenthal "USD" (sd) interaction and the van Hees-Glaudemans (fp) interaction, which were connected by the cross-shell Millener-Kurath interaction. Certain important two-body matrix elements and single-particle energies were adjusted to fit experimental binding energies in $A=40, 41, 42$. This interaction was then used to calculate level spectra for the daughter nuclei ^{35}S , ^{37}Cl , ^{38}Cl , and ^{38}Ar as well as Gamow-Teller and unique first-forbidden beta decays leading to these nuclei. The techniques used in these relatively large scale calculations are discussed in detail, as are the results.

I. INTRODUCTION

Our understanding of light nuclei via the shell model has made impressive progress in recent years. Particularly of note is the quite successful predictive power of effective one- and two-body interaction matrix elements based upon least-squares fits to the binding energies of nuclear levels. The success of this method was first evident from the work of Cohen and Kurath¹ for those levels of $A \leq 16$ best described as arising from $1s^4 1p^n$ configurations with $n \leq 12$. Even more detailed exploration of this technique was carried out by Wildenthal^{2,3} and his collaborators for nuclear levels best described by $1s^4 1p^{12} (2s, 1d)^n$ with $n \leq 24$. What is most extraordinary is the detailed success of these interactions in explaining observables other than the binding energies from which they are determined. The basic applicability of the shell model to nuclear structure cannot be displayed more transparently than by this success. For example, not only does the Wildenthal interaction for the $2s, 1d$ shell result in a successful detailed explanation of $M1$ and Gamow-Teller (GT) observables,^{4,5} but also the remaining systematic deviations between experiment and theory are close to those expected from fundamental considerations.⁶

What, then, is the next step in our understanding of

light nuclei via the shell model? Admittedly there are many problems still to tackle among $1s^4 1p^n$ and $1s^4 1p^{12} (2s, 1d)^n$ nuclei *per se*: however, a major obstacle to our understanding of light ($A < 50$) nuclei is a lack of knowledge of the interface between major shells at ^{16}O and at ^{40}Ca and of the related problem of ($\geq 2\hbar\omega$) intruder states in nuclei near these closed shells. An exploration of states with $A \sim 16$ describable by the lowest and next-to-lowest $1\hbar\omega$ particle-hole excitations allowable for a given N, Z combination has been made fairly successfully via the Millener-Kurath interaction;⁷ however, this interaction was based on a restricted form for the effective nucleon-nucleon potential and it is not as successful as might be expected for a more general form which is constrained to fit to binding energies. Several investigations have been initiated recently along this latter line.⁸⁻¹⁰

Our concern here is the interface between the ($2s, 1d$) and ($1f, 2p$) major oscillator shells, and, in particular, beta decay and electromagnetic observables between states involving sizable admixtures of both ($1f, 2p$) and ($2s, 1d$) configurations. Most shell-model studies at this interface and in the ($1f, 2p$) shell have been made in truncated configurational spaces. It has been amply demonstrated¹¹⁻¹³ that spin-dependent observables cannot be well reproduced in a space which does not include all spin-orbit partners;

here we make an attempt at some specific calculations in the full $(2s, 1d, 1f, 2p)$ configurational space.

Our testing ground is the beta decay of neutron-rich nuclei in the upper half of the $(2s, 1d)$ shell, specifically ^{35}P , ^{37}S , ^{38}S , and ^{38}Cl . In the next three sections we describe experimental investigations of these nuclear decays, and in Sec. V we return to the problems of describing these decays via the shell model.

It should be stated at the outset that we only observed two new β branches in these studies. Other than that, the principal contribution of the present experimental work is more accurate or corroborating intensity measurements for observed transitions and, most importantly, extraction of intensity limits for unobserved transitions. Unfortunately, previous investigators have been remiss in reporting such limits—which should be a routine part of any report on beta and gamma spectroscopy. Such limits are often nearly as informative as observed intensities in making comparisons to theory. In addition, they provide information of value for the planning of subsequent experiments.

Our present investigation also includes precision energy measurements of some of the more intense γ transitions. One motive for this effort is that these γ rays are produced copiously by fusion-evaporation reactions leading to $A \sim 35\text{--}38$ nuclei (see, e.g., Ref. 14) and they can provide useful energy calibration data in such studies.

II. BETA DECAY OF ^{37}S

A. Introduction

The beta decay of ^{37}S , illustrated in Fig. 1, was investigated previously by Hill,¹⁵ by Libert *et al.*,¹⁶ and by Raman *et al.*¹⁷ These investigations consisted of $\text{Ge}(\text{Li})$ spectroscopy of ^{37}Cl γ transitions following the decay of ^{37}S which has $t_{1/2} = 5.05(2)$ min (Ref. 18). In the first study by Hill,¹⁵ ^{37}S was formed by thermal neutron capture, $^{36}\text{S}(n, \gamma)^{37}\text{S}$, using 1 g samples of elemental sulfur or $(\text{NH}_4)_2\text{SO}_4$. The natural abundance of ^{36}S is only 0.017%. The $(\text{NH}_4)_2\text{SO}_4$ samples were subject to some chemical purification after the bombardment. In the study of Libert *et al.*,¹⁶ ^{37}S was produced by the $^{37}\text{Cl}(n, p)^{37}\text{S}$ reaction from bombardment of samples of natural CCl_4 and LiCl with 14.5-MeV neutrons from the $^3\text{H}(d, \alpha)n$ reaction. No chemistry was done.

Raman *et al.*¹⁷ carried out the most complete study of $^{37}\text{S}(\beta^-)^{37}\text{Cl}$. They used the (n, γ) reaction at the Los Alamos Omega West Reactor to form ^{37}S . Both ^{36}S samples (of the same material as used in the present studies) and natural S samples were bombarded. Seven transitions were observed with the same relative intensities with both samples and with half-lives of ~ 5 min. They were thus assigned to ^{37}S decay.

B. Relative γ -ray intensities

The present measurements were made in order to confirm these previous results with a different method of ^{37}S production and also to resolve some discrepancies in the three previous relative intensity measurements. The ^{37}S activity was formed by the $^{36}\text{S}(d, p)^{37}\text{S}$ reaction. The ^{36}S

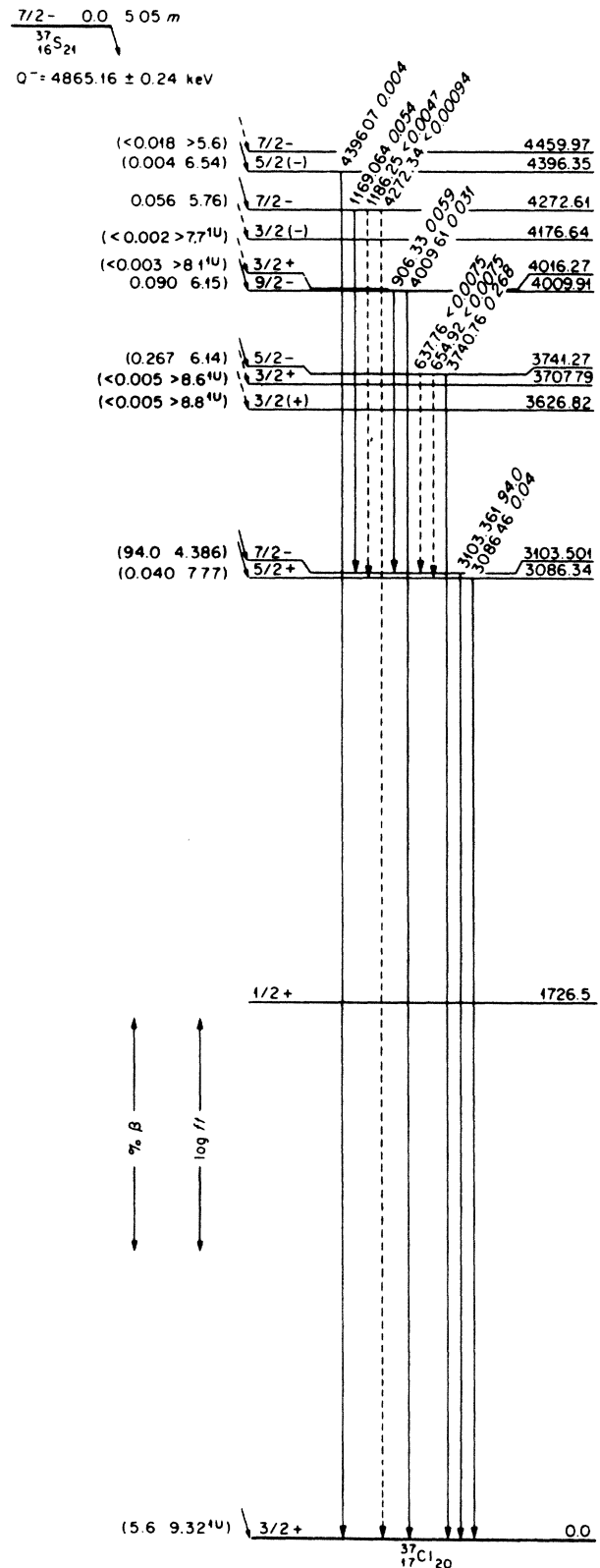


FIG. 1. Decay scheme for ^{37}S . The results are taken from those listed in the tables and discussed in the text. All energies are in keV. The numbers in parentheses to the left are the branching ratio (in %) and $\log f_0 t$ or $\log f_1 t$ (denoted by 1U). Spin and/or parity assignments in parentheses are not definite. The γ -ray transitions are labeled by their energies (not corrected for recoil) and relative intensities.

target consisted of a 0.0013-cm Ag foil sulfided with 300 $\mu\text{g}/\text{cm}^2$ of S enriched to 81.1% in ^{36}S . The target material and target manufacture were discussed previously.^{17,19} Two such targets were used for all the measurements reported herein. A "rabbit" target-transfer system²⁰ was used to transport the target between the bombard and count positions. Gamma rays were detected by an intrinsic coaxial Ge detector.

The ^{36}S target was bombarded by 100 nA of 3.0-MeV deuterons. The bombarding time was 1 min and the counting interval was 5 min. The Ge detector was separated from the rabbit by 0.6 cm of Lucite and 0.6 cm of lead at a distance of 3 cm. In 3.5 h, 40×10^6 counts were accumulated in a 4096-channel spectrum with a dispersion of 1.34 keV/channel. The spectrum obtained was quite similar in quality to that displayed in Ref. 17, albeit somewhat lower in statistics. The relative γ -ray efficiency, ϵ_γ , was assumed to have the form²¹

$$\epsilon_\gamma = A(E_\gamma^{-k} + B e^{-CE_\gamma}) \quad (1)$$

for $E_\gamma < 3.4$ MeV. The parameters of Eq. (1) were found from a least-squares fit to the intensities extracted from a ^{56}Co spectrum taken with an identical geometry. For $E_\gamma > 3.4$ MeV the γ -ray peak efficiency of Ge detectors deviates strongly from the E_γ^{-k} form established (in the present case) for $0.8 < E_\gamma < 3.4$ MeV. The efficiency decreases more rapidly with increasing E_γ than E_γ^{-k} . To estimate this effect in the present case, a $^{16}\text{N}(\beta^-)^{16}\text{O}$ γ -ray spectrum was accumulated under identical geometrical conditions. The known²² intensity ratio $I_\gamma(8.88 \rightarrow 6.13)/I_\gamma(6.13 \rightarrow 0)$ of 0.814(40)/69 was used to extract the relative efficiency at 2.74 and 6.13 MeV. A smooth curve was drawn joining the ^{56}Co and ^{16}N data. The efficiency determined in this manner at 4.01 MeV was $\approx 17\%$ lower than would result from an E_γ^{-k} extrapolation of the ^{56}Co data.

The intensity results from an analysis of this spectrum are compared to those of Refs. 15–17 in Table I. In this table and throughout this report, uncertainties in the least significant figure are in parentheses following the experi-

TABLE I. Gamma-ray energies, branching ratios (BR), and relative intensities in $^{37}\text{S}(\beta^-)^{37}\text{Cl}$. All data are from Refs. 17 or 20 unless otherwise noted. Except for column 1, the numbers in parentheses are the uncertainties in the least significant figure. The E_γ are not corrected for recoil and are from $E_i - E_f$ unless otherwise noted.

J_i^π ^a	E_i (keV)	E_f (keV)	E_γ (keV)	BR (%)	Relative Intensity ^b				
					Ref. 15	Ref. 16	Ref. 17	Present	Adopted
$\frac{5}{2}^+$	3086.34(18) ^c	0	3086.46(40) ^d	100			6.6(22)	2.8(18)	4.3(19)
$\frac{7}{2}^-$	3103.501(20) ^d	0	3103.361(20) ^d	100	10000	10000	10000	10000	10000
$\frac{3}{2}^{(+)}$	3626.82(6)	0	3625.63	57(2)			<0.3	<0.9	<0.3
		1727	1900.19	43(2)			<1.2	<9.0	<1.2
$\frac{3}{2}^+$	3707.79(9)	0	3707.59	73(3)			<0.4	<0.8	<0.4
$\frac{5}{2}^-$	3741.27(10) ^c	0	3740.76(30) ^d	100	23(2)	28(2)	27.6(28)	29.0(15)	28.5(11)
		3086	654.92	<1			<0.8	<2	<0.8 ^e
		3104	637.76	<1			<0.8	<2	<0.8 ^e
$\frac{9}{2}^-$	4009.91(10) ^c	0	4009.61(7) ^d	31(1)	1.8(4)	3.3(4)	2.9(11)	3.3(4)	3.3(3) ^f
		3104	906.33(7) ^d	69(1)	6.2(10)	6.3(4)	5.7(7)	6.4(3)	6.3(3) ^f
$\frac{3}{2}^+$	4016.27(9)	0	4016.04	33(3)			<0.1	<1.0	<0.1
		3086	929.92	48(3)			<0.6	<0.7	<0.6
$\frac{3}{2}^{(-)}$	4176.64(9)	0	1090.28	42(2)			<0.1	<1.0	<0.1
$\frac{7}{2}^-$	4272.61(8) ^c	0	4272.34	<2			<0.1	<1.0	<0.1
		3086	1186.25	3(1)			<0.5	<1.8	<0.5
		3104	1169.064(90) ^d	95(1)			5.0(7) ^g	6.3(6)	5.7(6)
$\frac{5}{2}^{(-)}$	4396.35(20) ^h	0	4396.07(20) ^h	98(1)			0.4(2)	<0.6	0.4(2)
$\frac{7}{2}^-$	4459.97(15)	3104	1373.60	43(1)				<1.9	<1.9

^aUncertain assignments are enclosed in parentheses.

^bRelative to 10000 units for the 3104-keV transition. The adopted value is the weighted mean of the present determination with those of Refs. 15 and 16.

^cWeighted average of the present determination with that of Ref. 17.

^dPresent determination (see text).

^eThese limits correspond to branching ratios of <3%.

^fThese intensities correspond to branching ratios for the 4010 \rightarrow 0 and 4010 \rightarrow 3104 transitions of 34(2)% and 66(2)%, respectively.

^gRevised value (M. E. Bunker, private communication).

^hReference 17.

mental value. The last column of Table I lists the weighted average of the last three determinations. The uncertainty of the weighted mean was multiplied by χ (normalized to the degrees of freedom) if $\chi^2 > 1$. Since there are no major discrepancies, we adopt these weighted means. The intensity results of Raman *et al.*¹⁷ are of higher statistics and consequently yield more stringent limits on unobserved transitions. However, for observed transitions their accuracy is mainly limited by the uncertainties in the efficiency calibration and for these transitions the present results are competitive.

The spin-parity assignments and γ -ray branching ratios listed for ^{37}Cl in Table I are mainly from the recent $^{36}\text{S}(p,\gamma)^{37}\text{Cl}$ studies of Nooren, de Esch, and van der Leun.²³ The energies corresponding to transitions not observed in the present work are also from this source. Decays to all ^{37}Cl levels with $E_x < 4.8$ MeV were considered, except the $J = \frac{1}{2}$ states¹⁸ at 1727 and 4269 keV. Throughout this report uncertain spin and/or parity assignments are placed in parentheses.

C. Gamma-ray energy measurements

Gamma-ray energies were measured for the six observed transitions in ^{37}Cl . The precision measurement for the 3103-keV transition will be described below. The other three values were obtained from the spectrum just

described. A crucial measurement was that of the 4010 \rightarrow 3104 transition which was greatly aided by the presence of $^{52}\text{Mn}(\beta^-)^{52}\text{Cr}$ γ rays produced via the $^{54}\text{Fe}(d,\alpha)^{52}\text{Mn}$ reaction in the iron backing of the ^{36}S target. The energies of these ^{52}Mn transitions are known to high precision²⁴ and provided a convenient internal calibration, the three most intense γ transitions having energies of 744.233(13), 935.544(12), and 1434.092(17) keV. Once the 4010 \rightarrow 3104 transition energy was known, it was used to calculate a value for the 4010 \rightarrow 0 transition energy. Then this latter transition provided a high-energy calibration point.

A careful measurement of the energy of the 3103-keV transition in ^{37}Cl was made with the mixed source technique. The procedures and precautions taken have been explained fully in previous descriptions of precision γ -ray energy measurements performed at this laboratory.^{20,25} Also, the same detector-amplifier-ADC (analog-to-digital converter) was used as in several previous measurements. Five spectra were recorded with mixed ^{37}S and ^{56}Co sources such that the full-energy peak of the ^{56}Fe γ transition of 3201.954(14) keV (Ref. 26) was of comparable intensity to that of the ^{37}Cl 3103-keV transition. A portion of one of these spectra is shown in Fig. 2. Each spectrum was recorded with a different ADC bias and amplifier gain. The average dispersion was ≈ 0.4 keV/channel. The five measurements gave excellent agreement, and the

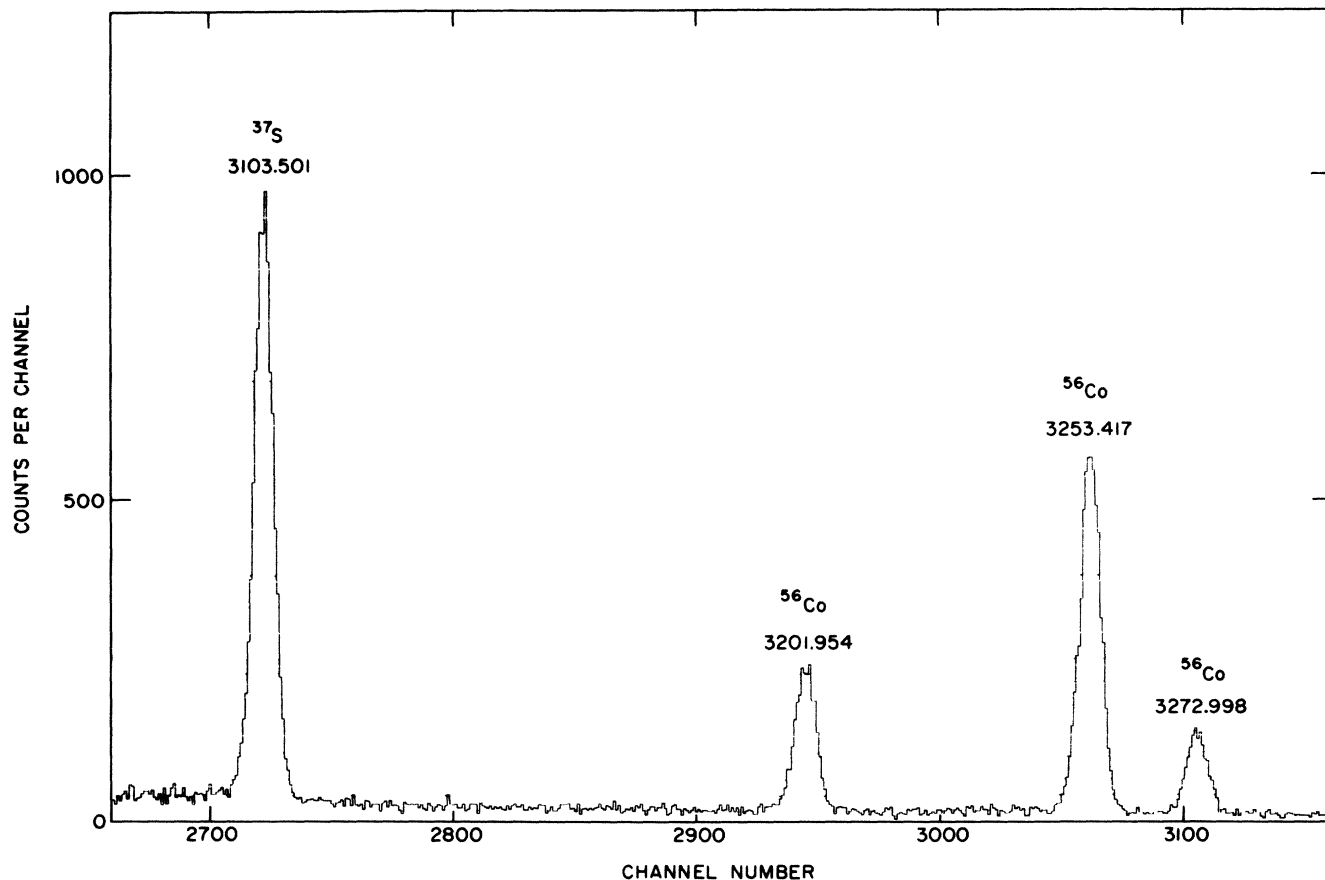


FIG. 2. Portion of one of five spectra taken with mixed ^{37}S - ^{56}Co activities. The energies of the γ -ray peaks are given in keV.

TABLE II. Comparison of ^{37}Cl excitation energies in keV.

Present	Ref. 23	Ref. 18
3086.34(18)	3086.12(7)	3086.6(4)
3103.501(20)	3103.59(8)	3103.3(2)
3741.27(10)	3741.05(15)	3740.9(5)
4009.91(10)	4011.3(6)	4010.6(5)
4272.61(8)	4272.52(17)	
4396.35(20)	4396.3(7)	4393.0(30)

weighted mean value for the difference in energy between the aforementioned two peaks was $\Delta(3202-3104) = 98.593(14)$ keV, which gives 3103.361(20) keV for the ^{37}Cl γ transition. Correcting for recoil gives 3103.501(20) keV for the excitation energy of the third-excited state of ^{37}Cl .

Our γ -ray energies, listed in column four of Table I, were used to derive level energies. The weighted average of our level energies and those of Raman *et al.*¹⁷ are listed in the second column of Table I. In Table II the ^{37}Cl excitation energies from $^{37}\text{S}(\beta^-)^{37}\text{Cl}$, i.e., the weighted mean of the present results with those of Raman *et al.*,¹⁷ are compared to those of Nooren *et al.*,²³ and to the adopted 1978 values of Endt and van der Leun.¹⁸ The agreement is seen to be satisfactory. Note that the 4273-keV level was independently discovered by Raman *et al.*¹⁷ and by Nooren *et al.*²³

D. Discussion

The γ -ray intensities of Table I were combined with a previous measurement²⁷ of the relative intensity for the g.s. β^- branch to obtain the β^- branching ratios of Table III. The ^{37}S g.s. has $J^\pi = \frac{7}{2}^-$ and thus all the decays listed in Table III—except that to the 4177-keV level—are allowed or first forbidden. The $\log f_n t$ values of Table III were calculated using the definitions and procedures of Warburton, Garvey, and Towner¹³ for allowed ($n=0$) and unique first-forbidden ($n=1$) decays. Note, however, that the decay to the $J^\pi = \frac{5}{2}^+$ 3086-keV level is nonunique, so that the energy weighting appropriate to unique decay is only correct if the rank 2 matrix element dominates the rank 1 matrix elements. A ^{37}S half-life¹⁸ of 5.05(2) min and the $Q(\beta^-)$ of 4865.16(24) keV from the 1983 Mass Table²⁸ were used in these calculations.

A comparison to theory is most conveniently made via the transition strength (matrix element squared) which we define as^{13,29,30}

$$B_n = 6166 \left\{ \frac{[(2n+1)!!]^2}{(2n+1)} \right\} \lambda_{\text{Ce}}^{2n} (f_n t)^{-1}, \quad (2)$$

where $2\pi\lambda_{\text{Ce}}$ is the Compton wavelength of the electron (386.159 fm). Equation (2) gives

$$B_0 = 6166/f_0 t, \quad 10^{-9} B_1 = 2758/f_1 t \text{ fm}^2. \quad (3)$$

TABLE III. Beta branches, $\log f_n t$ values, and transition strengths (B_n) for $^{37}\text{S}(\beta^-)^{37}\text{Cl}$ allowed Gamow-Teller ($n=0$) and first forbidden ($n=1$) decays.

$J_f^{\pi a}$	E_f (keV)	BR ^b (%)	n^a	$\log f_0 t^c$	$\log f_1 t^c$	B_n^d (fm ²ⁿ)
$\frac{3}{2}^+$	0	5.6(6)	1	7.54(5)	9.32(5)	1.32(14)
$\frac{5}{2}^+$	3086	0.040(21)	1 ^c	7.77(24)	8.77(24)	
$\frac{7}{2}^-$	3104	94.0(6)	0	4.386(4)		$254(2) \times 10^{-3}$
$\frac{3}{2}^{(+)}$	3627	<0.005	1	>8.0	>8.8	<4.8
$\frac{3}{2}^+$	3708	<0.005	1	>7.9	>8.6	<7.3
$\frac{5}{2}^-$	3741	0.267(11)	0	6.14(2)		$4.45(19) \times 10^{-3}$
$\frac{9}{2}^-$	4010	0.090(4)	0	6.15(2)		$4.33(20) \times 10^{-3}$
$\frac{3}{2}^+$	4016	<0.003	1	>7.6	>8.1	<23.0
$\frac{3}{2}^{(-)}$	4177	<0.002	(1)	>7.4	>7.7	<500 ^f
$\frac{7}{2}^-$	4273	0.056(6)	0	5.76(5)		$10.7(12) \times 10^{-3}$
$\frac{5}{2}^{(-)}$	4396	0.004(2)	0	6.54(22)		$1.8(9) \times 10^{-3}$
$\frac{7}{2}^-$	4460	<0.018	0	>5.6		< 13.5×10^{-3}

^aValues in parentheses are uncertain.

^bThe β^- branching ratio (BR) calculated using the ratio $\beta^-(\text{g.s.})/\beta^-(3104 \text{ keV}) = 0.059(6)$ of Ref. 27 and the adopted γ intensities of Table I.

^cThe $\log f_n t$ values defined in Ref. 13 calculated using $t_{1/2} = 5.05(2)$ min and $Q(\beta^-) = 4865.16(24)$ keV.

^dAllowed Gamow-Teller ($n=0$) and first-forbidden unique ($n=1$) transition strengths (matrix elements squared). See the text.

^eThis transition is nonunique.

^fAssuming $n=1$, i.e., $J^\pi = \frac{3}{2}^+$ for the 4177-keV level.

III. BETA DECAY OF ^{35}P

A. Introduction

The beta decay of ^{35}P has been observed following the $^{37}\text{Cl}(\gamma, 2p)^{35}\text{P}$ reaction,³¹ the $^{37}\text{Cl}(t, \alpha p)^{35}\text{P}$ reaction,³² the $^{18}\text{O}(^{19}\text{F}, 2p)^{35}\text{P}$ reaction,³³ and the $^{36}\text{S}(t, \alpha)^{35}\text{P}$ reaction.³³ The recommended¹⁸ half-life is 47.4(7) s. The beta endpoint, $Q(\beta^-)$, derived from recent $^{36}\text{S}(d, ^3\text{He})^{35}\text{P}$ energy measurements,^{19,34} is 3988.6(19) keV. The $(d, ^3\text{He})$ angular distributions of Refs. 19 and 34 also established the ^{35}P ground state as $J^\pi = \frac{1}{2}^+$. In the previous $^{35}\text{P}(\beta^-)^{35}\text{S}$ studies only one β^- branch to the $J^\pi = \frac{1}{2}^+$, 1572-keV first-excited state of ^{35}S was observed. Apt and Knight³² set the most stringent limits on decays to other excited states. These limits are all $< 0.45\%$. The aim of the present study was to search for weaker decays with a sensitivity ≥ 10 higher than this previous study.

B. Relative γ -ray intensities

^{35}P was produced by the $^{36}\text{S}(t, \alpha \gamma)$ reaction. The same rabbit-Ge system was used as in the $^{36}\text{S}(d, p)^{37}\text{S}(\beta^-)^{37}\text{Cl}$ study. A bombardment of ~ 100 nA of 3.4-MeV tritons for 40 s was followed by a 2 s transfer time and one to three 50 s counting intervals. The sensitivity for detecting weak branches was limited by the buildup of 5-min ^{37}S , 38-min ^{38}S , and 170-min ^{38}Cl activities. To mitigate this effect, two targets were used. Each was used for five bombard-count cycles and several hours elapsed before this 10-cycle schedule was repeated. One new ^{35}P β^- branch was observed; namely, decay to the ^{35}S 2938-keV level, which was previously known to γ decay $\sim 100\%$ to the ^{35}S ground state.^{18,35} The ground-state transitions

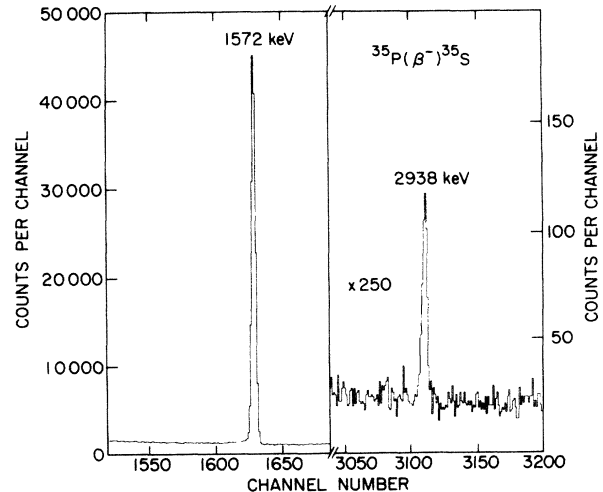


FIG. 3. Portion of Ge spectrum showing the two observed γ transitions from ^{35}P β^- decay. The 2938-keV transition has an intensity relative to that of the 1572-keV transition of 0.476(30)%.

from the ^{35}S 1572- and 2938-keV levels are illustrated in Fig. 3. The energy of the 2938-keV transition was measured to be 2938.29(40) keV, corresponding to an excitation energy of 2938.42(40) keV. Previous values for this energy are 2939.2(13) keV (Ref. 18) and 2938.64(11) keV (Ref. 35). This new transition was associated with ^{35}P decay on the basis of (1) its half-life, which was consistent ($\pm 10\%$ uncertainty) with the expected value of 47 s, and (2) its agreement in energy with the expected^{18,35} decay of

TABLE IV. Beta branching ratios (BR), $\log_{10} t$ values, and Gamow-Teller strengths (B_0) for $^{35}\text{P}(\beta^-)^{35}\text{S}$ decay. The theoretical (theor.) B_0 values are the effective values of Ref. 4.

$J_f^{\pi a}$	E_f (keV)	BR ^b (%)	$\log_{10} t$	B_0 (expt.)	B_0 (theor.)
$\frac{3}{2}^+$	0	(0.73) ^c	(7.214) ^c		4.21×10^{-4}
$\frac{1}{2}^+$	1572	98.80(3)	4.125(7)	0.462(7)	0.518
$\frac{7}{2}^-$	1991	< 0.08	> 6.8		
$\frac{3}{2}^-$	2348	< 0.08	> 6.5		
$\frac{5}{2}^+$	2717	< 0.03	> 6.5		
$\frac{3}{2}^+$	2938	0.47(3)	4.96(3)	0.067(4)	0.091
$\frac{5}{2}^+$	3421	< 0.02	> 5.3		
$[\frac{3}{2}^-, \frac{5}{2}^-]$	3558	< 0.11	> 4.1		
$[\frac{7}{2}^+]$	3597	< 0.02	> 4.8		
$[\frac{1}{2}^-, \frac{3}{2}^-]$	3675	$< 0.02^d$	$> 4.4^d$		
$\frac{3}{2}^-$	3802	< 0.03	> 3.4		

^aSpin-parity assignments in square brackets are our speculations—see Sec. V B 4.

^bCalculated from the γ branches of Refs. 18 and 35.

^cCalculated from the listed theoretical value of B_0 and assumed in obtaining the other branching ratios.

^dThe γ branching of the 3675-keV level has not been measured. This limit corresponds to an assumed 100% ground-state branch.

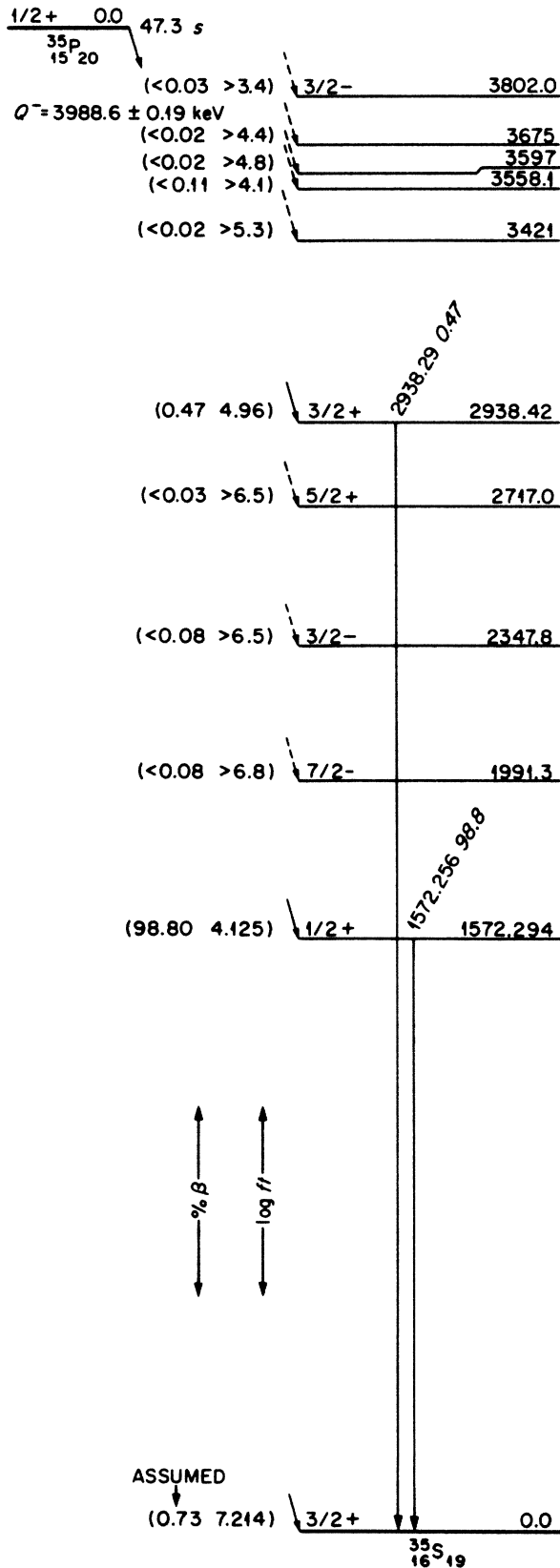


FIG. 4. Decay scheme for ^{35}P . The $^{35}\text{P}(\beta^-)^{35}\text{S}$ g.s. branching ratio is the theoretical prediction (see text). See the caption of Fig. 1 for further details.

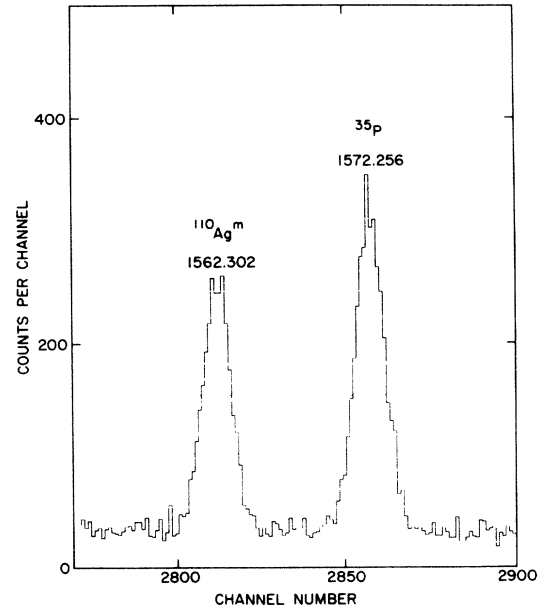


FIG. 5. Portion of one of four spectra taken with mixed ^{35}P - $^{110}\text{Ag}^m$ activities. The energies of the γ -ray peaks are given in keV.

the 2938-keV level of ^{35}S . Relative γ -ray intensities were obtained with the aid of a ^{56}Co calibration. Results for the two observed transitions and limits derived from unobserved ones are summarized in Table IV. The beta decay of ^{35}P is illustrated in Fig. 4.

C. Gamma ray energy measurements

The energy of the 1572-keV γ ray was measured relative to the $^{110}\text{Ag}^m$ γ ray of 1562.302(5) keV (Ref. 26). Other $^{110}\text{Ag}^m$ γ rays provided secondary standards. Four measurements were made; all were in good agreement and yielded $\Delta(1572 - 1562) = 9.954(23)$ keV. A portion of one of these spectra is illustrated in Fig. 5. We adopt 1572.256(24) keV for the energy of the ^{35}S $1572 \rightarrow 0$ γ ray. This corresponds to an excitation energy of 1572.294(24) keV for the first-excited state of ^{35}S . Previous values for this excitation energy are 1572.28(13) keV (Ref. 18) and 1572.298(33) keV (Refs. 35 and 36).

IV. BETA DECAY OF ^{38}S

A. Introduction

Previous investigations of $^{38}\text{S}(\beta^-)^{38}\text{Cl}$ and the subsequent decay of ^{38}Cl to ^{38}Ar were made by Nethaway and Caretto,³⁷ who first observed ^{38}S decay, by Engelbertink and Olness,³⁸ and by Visser and Lindner.³⁹ The adopted half-lives¹⁸ and β^- Q values²⁸ are 170.3(7) min and 2936(12) keV for ^{38}S decay and 37.24(5) min and 4916.5(8) keV for ^{38}Cl decay. The ^{38}S - ^{38}Cl decay schemes are illustrated in Fig. 6.

Engelbertink and Olness³⁸ produced ^{38}S via $^{36}\text{S}(t,p)^{38}\text{S}$ on 1.93% enriched sulfur. They detected γ rays with a bare 30-cm³ Ge(Li) detector. Visser and Lindner³⁹ pro-

duced ^{38}S via the $^{40}\text{Ar}(\gamma,2p)^{38}\text{S}$ reaction. They performed chemical separation of the sulfate and, for some measurements, continuous "on-line" separation of the ^{38}S and ^{38}Cl activities. They detected γ rays with both bare and CSS (Compton suppression spectrometer) Ge detectors. The combination of chemical purification and CSS spectrometry gave their experiment unusually high sensitivity and they reported two γ transitions from $^{38}\text{S}(\beta^-)^{38}\text{Cl}$ not observed by Engelbertink and Olness.³⁸

Our main motivation in the present study was to verify the results of Visser and Lindner³⁹ and to set limits on other unobserved transitions. In addition, some effort was

spent on precision energy measurements of the three most intense γ rays from ^{38}S - ^{38}Cl decay.

B. Relative γ -ray intensities

The γ spectra of ^{38}S - ^{38}Cl in equilibrium was recorded with a CSS detector consisting of a NaI(Tl) annulus and an intrinsic coaxial, 100-cm³ Ge detector. The ^{36}S target was bombarded for 2–3 h with 250 nA of 3.1-MeV tritons. After a waiting period of ~ 3 h, a spectrum was recorded for from 1–10 h. Approximately 20 h total counting time was collected from four bombardments. Analysis of the resulting spectrum resulted in the γ intensities of Table V.

C. Gamma-ray energy measurements

Precision energy measurements of γ transitions following ^{38}S - ^{38}Cl β decay were made via the mixed source technique. The preparation of the ^{38}S - ^{38}Cl sources was as described in the preceding subsection. The reference γ rays were provided by ^{56}Co and ^{144}Ce sources²⁶ and ^{20}F decay.⁴⁰ The latter activity has a half-life of 11 s. It was produced by the $^{19}\text{F} + d$ reaction and the "rabbit" system was used to present ^{20}F activity with minimum background. Precautions²⁵ were taken to avoid systematic uncertainties, associated with the use of a short-lived energy standard. The results of these precision energy measurements are summarized in Table VI. An example of the data is shown in Fig. 7.

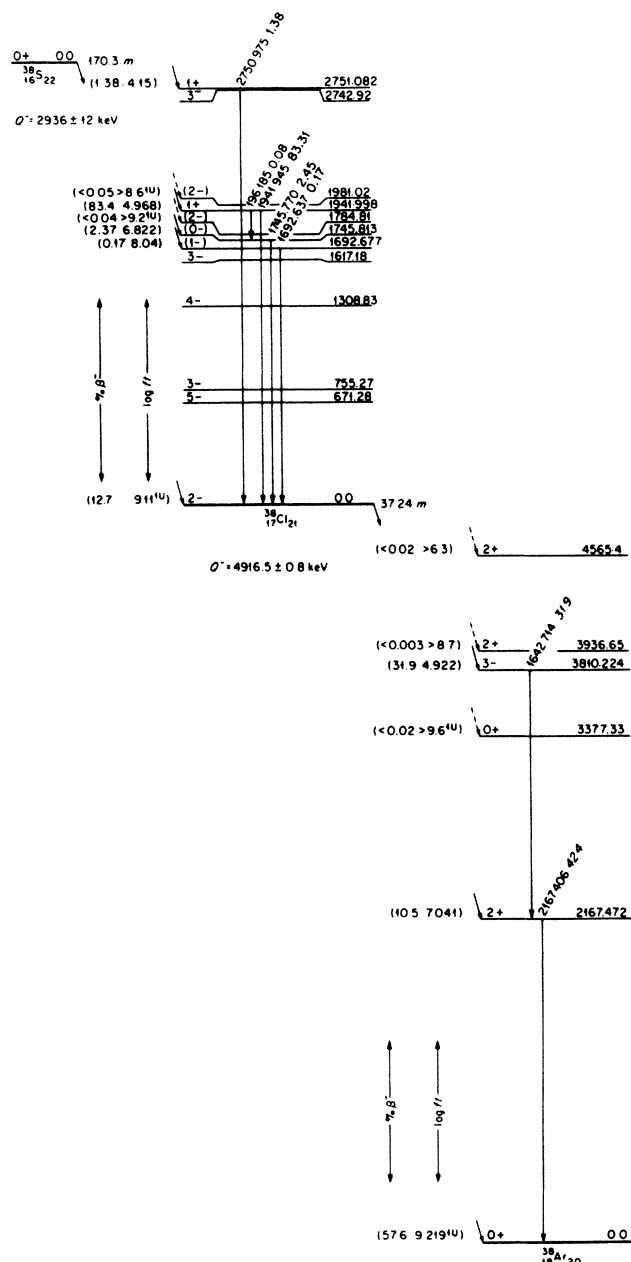


FIG. 6. Decay schemes of ^{38}S and ^{38}Cl . See the caption of Fig. 1 for details.

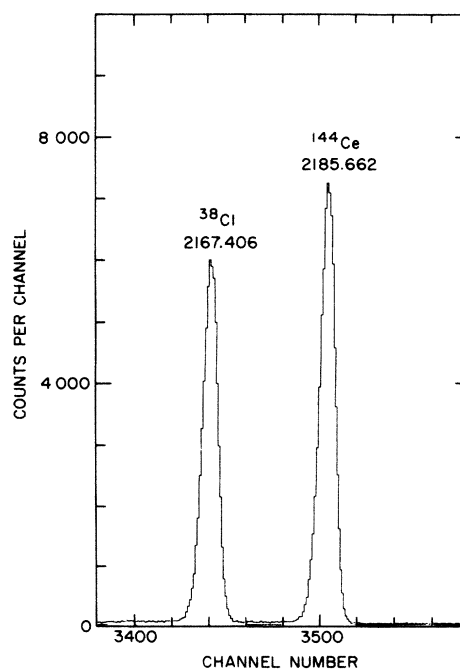


FIG. 7. Portion of one of 13 spectra taken with mixed ^{38}S - ^{38}Cl - ^{144}Ce activities. The energies of the γ -ray peak are given in keV.

TABLE V. Gamma-ray energies, branching ratios (BR), and relative intensities from ^{38}S - ^{38}Cl in equilibrium.

$J_i^{\pi a}$	E_i^b (keV)	E_f (keV)	E_{γ}^b (keV)	BR ^c (%)	e	Relative Intensity ^d f	Present	Adopted
$^{38}\text{S}(J^{\pi}=0^+) \rightarrow ^{38}\text{Cl}$								
(1 ⁻)	1692.677(80)	0	1692.637(80)	92.6(14)	< 50		20(2)	20(2)
(0 ⁻)	1745.813(40)	0	1745.770(40)	100	340(40)	260(30)	295(8)	294(9)
(4 ⁻)	1784.81(17)	755	1029.52(17)	100	< 50		< 4	< 4
1 ⁺	1941.998(14)	1746	196.185(40) ^g	0.10(3)		20(7)	9(2)	10(3)
		0	1941.945(14)	99.90(3)	10 000	10 000	10 000	10 000
(2 ⁻)	1981.02(10)	0	1980.96(10)	43.7(7)	< 50		< 6	< 6
1 ⁺	2751.082(70)	0	2750.975(70)	100		190(20)	164(5)	166(6)
$^{38}\text{Cl}(J^{\pi}=2^-) \rightarrow ^{38}\text{Ar}$								
2 ⁺	2167.472(9)	0	2167.406(9)	100	6500(100)	6400(100)	6630(100)	6510(100)
0 ⁺	3377.33(12)	2167	1209.84(12)	99.34(10)	< 24 ^h		< 3	< 3
3 ⁻	3810.224(18)	2167	1642.714(16)	99.928(8)	4800(100)	4700(100)	4950(100)	4817(100)
2 ⁺	3936.65(18)	0	3936.43(18)	93.8(7)	< 0.4 ^h		< 1	< 0.4
2 ⁺	4565.4(2)	2167	2397.9(2)	96.0(4)	< 3 ^h		< 3	< 3

^aThe J^{π} values in parentheses are based partly on shell-model predictions (see Sec. V). The others are from Ref. 18.

^bIf the γ -ray decay of a level was not observed, then E_i is from Ref. 18 and E_{γ} from $E_i - E_f$. For observed transitions E_i and E_{γ} are from the present results, unless noted otherwise. E_i is corrected for recoil, E_{γ} is not.

^cAll branching ratios (BR) are from Ref. 18, except for that of the ^{38}Cl 1942-keV level, which is from the results in this table, and the ^{38}Cl 2751 \rightarrow 0 transition, which is assumed to be 100% and for which a limit of < 5% was placed on any other branch (Ref. 39).

^dRelative to 10 000 units for the ^{38}Cl 1942 \rightarrow 0 transition. The adopted values are the weighted mean of the three determinations.

^eReference 38 unless otherwise noted.

^fReference 39.

^g E_{γ} is from $E_i - E_f$.

^hThe limits were inferred from those given for $\log f_0 t$ by Ref. 41.

D. Analysis

1. $^{38}\text{S}(\beta^-)^{38}\text{Cl}$

As shown by Engelbertink and Olness,³⁸ the β^- branch of ^{38}S to the ^{38}Cl ground state can be determined from the intensity balance of the ^{38}S γ -ray flux into the ^{38}Cl ground state, the intensity of the $^{38}\text{Cl}(\beta^-)^{38}\text{Ar}$ 2167-keV γ ray (in equilibrium), and the known⁴¹ branching ratio of 57.6(13)% for ^{38}Cl to the ^{38}Ar ground state. The very small ^{38}Ar 3810 \rightarrow 0 branch can be accounted for, but is of negligible importance. Applying the appropriate relationship³⁸ for sequential decays in equilibrium to the adopted intensities of Table V, we obtain 12.7(32)% for the $^{38}\text{S}(\beta^-)^{38}\text{Cl}$ (g.s.) branch. The remaining ^{38}S branching ratios were routinely calculated from the adopted intensities of Table V and are given in Table VII.

One new branch was observed in $^{38}\text{S}(\beta^-)^{38}\text{Cl}$, namely

that to the 1693-keV level. The half-life associated with the 1693-keV transition was measured to be 200(\sim 60) min, in reasonable agreement with the value expected for ^{38}S decay, which is 170 min. Our measured energy for the 1693 \rightarrow 0 transition differs by +457(130) eV from the previous most accurate value of Spits and Akkermans.⁴² This difference is consistent with a similar discrepancy of +293(140) eV for the nearby 1746 \rightarrow 0 transition.

2. $^{38}\text{Cl}(\beta^-)^{38}\text{Ar}$

The branching ratios for ^{38}Cl β^- decay were obtained assuming the 57.6(13)% g.s. branch of van Klinken *et al.*⁴¹ and a best value for the intensity ratio of the 1643- and 2167-keV transitions. This best value was the weighted average of the three ratios from Table V, the value of Ref. 41, and that of Spits and Akkermans.⁴² The resulting branching ratios are listed in Table VIII.

TABLE VI. Results of precision energy measurements for γ rays observed following ^{38}S decay.

Daughter nucleus	E_{γ} (keV)	Reference line (keV)	Number of measures	$\Delta(E_{\text{ref}} - E_{\gamma})$ (keV)
^{38}Ar	2167.406(9)	^{144}Ce 2185.662(7)	13	18.256(5)
^{38}Ar	1642.721(17)	^{20}F 1633.602(15)	5	-9.119(7)
^{38}Ar	1642.700(18)	^{56}Co 1771.350(15)	4	128.650(10)
^{38}Ar	1642.714(16)	Adopted value		
^{38}Cl	1941.945(14)	^{56}Co 1963.714(12)	4	21.769(7)

TABLE VII. Beta branches, $\log f_n t$ values, and transition strengths (B_n) for $^{38}\text{S}(\beta^-)^{38}\text{Cl}$ allowed ($n=0$) and first forbidden ($n=1$) decays.

$J_f^{\pi a}$	E_f (keV)	BR (%)	n	$\log f_0 t$	$\log f_1 t$	B_n^b (fm^{2n})
2^-	0	12.7(32)	1	7.73(11)	9.11(11)	2.12(54)
(1^-)	1692	0.17(2)	1	8.04(5)	8.78(5)	
(0^-)	1745	2.37(11)	1	6.822(28)	7.523(32)	
(2^-) ^c	1785	<0.04	1	>8.5	>9.2	<1.31
1^+	1942	83.4(30)	0	4.968(25)		0.0664(39)
(2^-)	1981	<0.05	1	>8.1	>8.6	<6.0
1^+	2751	1.38(7)	0	4.15(10)		0.44(9)

^aThe values in parentheses are chosen from the possibilities allowed by Endt and Van der Leun (Ref. 18) on the basis of shell-model predictions.

^bAllowed Gamow-Teller ($n=0$) and first-forbidden unique ($n=1$) transition strength (matrix elements squared). See the text.

^cThe predicted spin of this level is 4 (see Sec. V). The results are included because $J=2$ is not ruled out experimentally.

V. SHELL MODEL CALCULATIONS

A. The interaction

The starting point for our $2s, 1d, 1f, 2p$ interaction—labeled SDPF—is the “universal” $2s, 1d$ interaction—denoted USD—of Wildenthal.³ The parameters of this interaction consist of 63 two-body matrix elements (2BME’s) and three single-particle energies (SPE’s) relative to the ^{16}O core. There are 510 2BME’s and four SPE’s necessary to fully describe the cross-shell interaction, i.e., that connecting the $2s, 1d$ and $1f, 2p$ shells. Several different sets of cross shell 2BME’s were generated from effective nucleon-nucleon potentials as well as from a modified-surface-delta interaction (MSDI). The potentials used were Schiffer-True,⁴³ the density dependent Skyrme interaction labeled SGII,⁴⁴ and the Millener-Kurath (MK) potential.⁷ The MSDI interaction used was that of van der Poel.^{23,45} Of these the most successful was the Millener-Kurath potential,⁷ which we then adopted. The vast majority of the 2BME’s generated from the

Millener-Kurath potential were left unchanged. However, for present purposes, the most important cross-shell 2BME’s are the eight $\langle d_{3/2} f_{7/2} | V | d_{3/2} f_{7/2} \rangle$ with $J=2-5$ and $T=0-1$. As a first iteration, these were modified such that the binding energies of the lowest-lying ^{40}Ca $T=0$ and $T=1$ 2^- , 3^- , 4^- , and 5^- levels were reproduced essentially exactly (within ~ 10 keV). In this and all subsequent iterative adjustments, the SPE’s of the $f_{7/2}$, $f_{5/2}$, $2p_{3/2}$, and $2p_{1/2}$ orbits were adjusted so that the excitation energies of the lowest-lying $\frac{7}{2}^-$, $\frac{5}{2}^-$, $\frac{3}{2}^-$, and $\frac{1}{2}^-$ levels of ^{41}Ca were fixed to be 0, 6.90, 2.07, and 4.13 MeV, respectively, with the ^{41}Ca - ^{40}Ca separation energy constrained as 8.363 MeV (the experimental value).

The validity of fitting to the ^{40}Ca $T=0$ and $T=1$ 2^- - 5^- quadruplets in this manner depends on their having dominant $d_{3/2} f_{7/2}$ character. A measure of the intensity of $d_{3/2} f_{7/2}$ in their wave functions is provided by the $l=3$ spectroscopic factors S_p^+ for $^{39}\text{K} + p$ and S_n^+ for $^{39}\text{K} + n$. In Table IX we list the “best values” of these factors as evaluated by Endt,⁴⁶ along with the predictions of our calculations. In Table IX MK refers to the

TABLE VIII. Beta branches, $\log f_n t$ values, and transition strengths (B_n) for $^{38}\text{Cl}(\beta^-)^{38}\text{Ar}$ allowed ($n=0$) and first forbidden ($n=1$) decays.

J_f^{π}	E_f (keV)	BR (%)	n	$\log f_0 t$	$\log f_1 t$	B_n^a (fm^{2n})
0^+	0	57.6(13) ^b	1	7.426(10)	9.219(10)	1.67(4)
2^+	2167	10.5(3) ^c	1	7.041(12)	8.373(12)	
0^+	3377	<0.02	1	>8.7	>9.6	<0.71
3^-	3810	31.9(10) ^c	0	4.922(14)		0.0738(23)
2^+	3937	<0.003	1	>8.7	>9.3	
2^+	4565	<0.02	1	>6.3	>6.2	

^aAllowed Gamow-Teller ($n=0$) and first-forbidden unique ($n=1$) transition strength (matrix elements squared). See the text.

^bReference 41.

^cThe total branching ratio for excited states is taken from Ref. 41, 42.4(13)%. The ratio of the branches to the 2167- and 3810-keV levels was taken as the weighted average of the three determinations of Table V, with those of Refs. 41 and 42.

TABLE IX. The $l=3$ spectroscopic factors for ^{40}Ca and ^{40}K .

J^π, T	Expt. ^a	S^+			Expt.	E_x (keV)	
		MK	MK(exact)	SDPF		MK	SDPF
$2_1^-, 0$	0.24(4)	0.91	0.96	0.96	6026	7540	6035
$2_2^-, 0$	0.44(8)	0.02	0.01	0.01	6751	8430	8419
$3_1^-, 0$	0.55(6)	0.36	0.75	0.60	3737	4850	4393
$3_2^-, 0$	<0.01	0.25	0.17	0.23	6285	6780	6530
$4_1^-, 0$	0.91(10)	0.97	0.98	0.99	5614	6573	5624
$5_1^-, 0$	0.84(9)	0.93	0.93	0.93	4492	4990	4501
$2_1^-, 1$	0.77(9)	0.91	0.93	0.93	8424	8832	8435
$3_1^-, 1$	0.96(12)	0.96	0.96	0.96	7695	7711	7706
$4_1^-, 1$	0.94(14)	0.99	0.99	0.99	7659	7634	7667
$5_1^-, 1$	0.88(10)	0.99	0.99	0.99	8551	8300	8559

^aReference 46.

Millener-Kurath potential⁷ and MK("exact") to the modification of MK just described. In a pure $d_{3/2}f_{7/2}$ model the spectroscopic factors for the four $T=0$ 2_1^- – 5_1^- states and four $T=1$ 2_1^- – 5_1^- states are unity. The experimental S^+ are consistent with six of the eight 2_1^- – 5_1^- yrast $T=0$ and yrast $T=1$ levels being dominantly $d_{3/2}f_{7/2}$, but not the $T=0$ 2_1^- and 3_1^- levels. The calculations do a fair job of reproducing S^+ for the $(J_i^\pi, T)=(3_1^-, 0)$ level, but not the $(2_1^-, 0)$ level. Here, J_i^π denotes the i th level (ordered by excitation energy) of the given J^π . As we now explain, some attempt was made to improve the agreement of the S^+ for both these levels.

It is well known that collective effects selectively lower the energies of low-lying 3^- states in even-even nuclei. Thus the $(3_1^-, 0)$ particle-hole matrix element was changed to about midway between the MK value and the empirical ^{40}Ca value, with the consequence that the predicted 3^- excitation energy was 668 keV too high. This change brought the predicted spectroscopic factor for this state into somewhat better agreement with experiment. The resulting interaction is labeled SDPF in Table IX. A similar procedure had little effect on the S^+ for the $(2_1^-, 0)$ and $(2_2^-, 0)$ levels and so no change was made in the $(2, 0)$ particle-hole matrix element. The very poor prediction of the SDPF interaction for the excitation energy of the $(2_2^-, 0)$ level (see Table IX) is probably a clue to the difficulty. Better agreement can only be achieved by adjustments of other 2BME's—such as the $\langle d_{3/2}p_{3/2} | V | d_{3/2}p_{3/2} \rangle$ —and this we do not wish to undertake at this time. We shall proceed with the cross-shell interaction just described, but shall keep the noted discrepancy for the $(2^-, 0)$ states in mind.

Only the 195 2BME's for the fp interaction remain to be determined. The starting point for this set was the effective interaction of van Hees and Glaudemans.⁴⁷ These authors determined an interaction from a least squares fit to binding energies in the $A \sim 51$ – 55 region using a model space of $f_{7/2}, p_{3/2}, p_{1/2}, f_{5/2}$, but with only zero or one particle allowed out of the $f_{7/2}$ orbit. In the present study, the extra 2BME's needed for an unrestricted fp space were generated from the MSDI using the parameters $(A_1, A_0, B_1, B_0) = (0.25, 0.53, -1.09, 0.50)$ MeV (Ref. 48).

For the present application the most important of the

195 fp 2BME's are the eight $\langle f_{7/2}f_{7/2} | V | f_{7/2}f_{7/2} \rangle$ matrix elements. These were adjusted iteratively until the binding energies (relative to ^{40}Ca) of the lowest-lying $J=0$ – 7 levels of ^{42}Sc (J odd) and ^{42}Ca (J even) matched experiment.¹⁸ All the 2BME's were evaluated for $A=40$ and then assumed to vary as $(40/A)^{0.3}$. This is the same mass dependence used in the USD, and seems to be a reasonable approximation to that expected for harmonic oscillator 2BME's based on a realistic G matrix.⁴⁹

Our calculations will be performed in the model spaces $(sd)^{40-16-n}(fp)^n$. We shall refer to these spaces as $n\hbar\omega$ excitations. In general, we shall consider the two lowest allowed $n\hbar\omega$ excitations in order to obtain the low-lying even and odd parity spectra. In many cases it would be instructive to include $(n+2)\hbar\omega$ and even higher excitations in our $n\hbar\omega$ model space. Because of dimensional restrictions, calculations in such model spaces are generally beyond our present capabilities. Moreover, calculations done for ^{38}Ar in a truncated space indicated that our SDPF interaction is not suitable for calculating binding energies in a mixed $0\hbar\omega + 2\hbar\omega$ configurational space. This is an old and extremely difficult problem encountered in all attempts to explain mixed cross-shell spectra or even mixed subshells⁵⁰ such as $f_{7/2}^n p_{3/2} + f_{7/2}^{n-1} p_{3/2}^2$ (Refs. 51 and 52). The difficulty is that the $2\hbar\omega$ states, which have similar symmetries to the low-lying $0\hbar\omega$ states, lie at high energy but still interact strongly and push the $0\hbar\omega$ states considerably lower in energy. If we included $4\hbar\omega$ states, then a similar effect would push down the low-lying $2\hbar\omega$ states and approximately restore the "correct" relative binding energies. Unfortunately, dimensional restrictions preclude inclusion of $4\hbar\omega$ states and, in any case, the series is very slowly converging. We shall discuss this difficulty further when we consider unique first-forbidden beta decays in Sec. V D. It should be remembered that it is a fundamental property of effective interactions that the $n\hbar\omega$ model space can adequately account for admixtures of $(>n)\hbar\omega$ components of all types.⁵³

In the nuclei just below $A=40$ there are low-lying $(\geq n+2)\hbar\omega$ intruder states. These states tend to be deformed while the $n\hbar\omega$ states are more nearly spherical. The low-lying $n\hbar\omega$ and $(\geq n+2)\hbar\omega$ states do not mix very strongly, but it is important to identify them in order

to understand these nuclei. For this reason we have also carried out calculations using an effective $d_{3/2}f_{7/2}$ interaction (denoted WDF) developed by Wildenthal⁵⁴ for just such a purpose. For all four nuclei the calculation for both even and odd parity states were performed in the full $(d_{3/2}f_{7/2})^{4-32}$ space, e.g., ^{38}Ar $\pi = +$ states include $0\hbar\omega$, $2\hbar\omega$, $4\hbar\omega$, and $6\hbar\omega$ terms.

Our calculations were done with the computer program OXBASH.⁵⁵ OXBASH works in the m scheme but utilizes projected basis vectors which have good J and T . With the computer resources available to us we can handle J, T states with dimensions up to 2500 to ~ 3000 and m -scheme dimensions up to 75 000, depending on the number of partitions. For calculations with larger J, T dimension, some sort of truncation was necessary. Several different options exist in OXBASH. These are (1) limitations on specific subshell occupancies, (2) limitations on the number of unpaired nucleons denoted by S , and (3) limitation to a specific list of allowed partitions. A partition is a specific occupancy of the seven subshells of SDPF. Thus, both (1) and (2) pick certain classes of partitions. We shall list partitions and subshell occupancies in the form $[n(d_{5/2}), n(d_{3/2}), n(s_{1/2}); n(f_{7/2}), n(f_{5/2}), n(p_{3/2}), n(p_{1/2})]$, where $n(j)$ denotes the number of nucleons in the subshell j . In these calculations spuriousity was removed using the method of Gloeckner and Lawson.⁵⁶

B. Energy levels

As a first test of the interaction, we consider energy level spectra for the daughter nuclei of the current β^- decay study. We are interested in nuclear levels involving particles in both the sd and fp shells. As summarized in Table X, the dimensions of the matrices which must be diagonalized in order to obtain the wave functions increase rapidly for a given $n\hbar\omega$ as A departs from 40. Thus, we consider the nuclei of interest in the order ^{38}Ar , ^{38}Cl , ^{37}Cl , and ^{35}S .

1. ^{38}Ar

Our calculated spectra for ^{38}Ar is compared to experiment in Fig. 8.

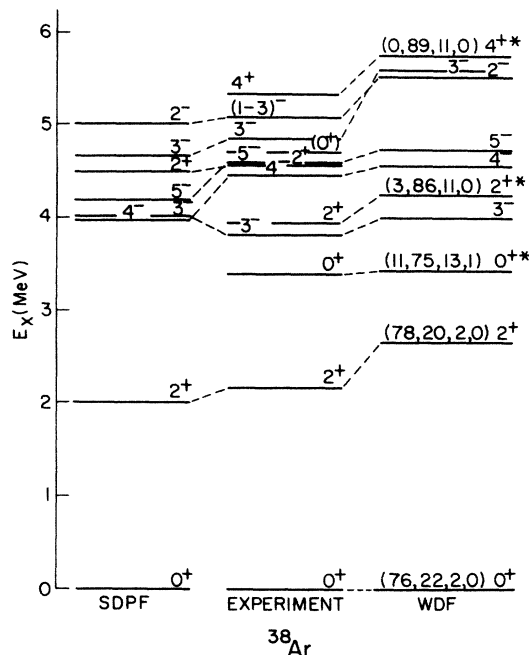


FIG. 8. Comparison of the calculated and experimental level schemes of ^{38}Ar . The experimental data are from Ref. 18. All known states below 5.4 MeV are included. The percentages of $0\hbar\omega$, $2\hbar\omega$, $4\hbar\omega$, and $6\hbar\omega$ in the $\pi = +$ WDF wave functions are given in parentheses, and predominantly $2\hbar\omega$ states are labeled by asterisks.

a. The WDF calculation. We discuss two cases.

Even parity. The WDF calculation in the $(d_{3/2}f_{7/2})^6$ model space is shown to the right in Fig. 8. For the even-parity states the intensity in the wave functions of $0\hbar\omega$, $2\hbar\omega$, $4\hbar\omega$, and $6\hbar\omega$, respectively, is given in parentheses. The predominantly $2\hbar\omega$ intruder states are marked by an asterisk. There is ample experimental evidence that the 0^+ 3.38-MeV level, 2^+ 3.94-keV level, and 4^+ 5.35-MeV level are $\geq 2\hbar\omega$ intruder states (see, e.g., Refs. 57 and 58). It is clear that the 0_2^+ , 2_2^+ , and 4_1^+ levels of ^{38}Ar are nicely accounted for by the WDF interaction which identifies them as $2\hbar\omega$ states.

TABLE X. Dimensions of the J matrices for the lowest two $n\hbar\omega$ SDPF model spaces for ^{38}Ar , ^{38}Cl , ^{37}Cl , and ^{35}S .

Nucleus	configuration	J						
		0	1	2	3	4	5	6
^{38}Ar	$(sd)^{22}$	3	2	5	2	2	0	0
	$(sd)^{21}(fp)$	105	287	394	411	353	256	157
^{38}Cl	$(sd)^{21}(fp)$	31	87	119	121	102	72	41
	$(sd)^{20}(fp)^2$	2318	6582	9626	10 897	10 574	9094	6930
Nucleus	configuration	J						
		$\frac{1}{2}$	$\frac{3}{2}$	$\frac{5}{2}$	$\frac{7}{2}$	$\frac{9}{2}$	$\frac{11}{2}$	$\frac{13}{2}$
^{37}Cl	$(sd)^{21}$	5	10	10	6	5	1	0
	$(sd)^{20}(fp)$	564	993	1201	1279	984	709	441
^{35}S	$(sd)^{19}$	75	129	148	136	103	64	33
	$(sd)^{18}(fp)$	4995	8937	11 253	11 717	10 594	8487	6051

Odd parity. All odd-parity states predicted by the WDF calculation below 6-MeV excitation are $< 78\%$ $1\hbar\omega$ with the $3\hbar\omega$ states calculated to commence at ~ 7350 keV with $J^\pi=7^-$. Experimentally, the lowest 7^- state known is at 7508 keV (Ref. 18).

b. The SDPF calculation. We discuss two cases.

Even parity. The even-parity states were calculated in the $0\hbar\omega$ model space, i.e., $(sd)^{22}$, and are thus just those of the USD interaction.⁵⁹

Odd parity. The $1\hbar\omega$ states utilize our SDPF interaction. Granting a 2^- assignment for the 5084-keV level, there is a one-to-one correspondence between the experimental and calculated odd-parity states below 5.4-MeV excitation. The average rms deviation for the five odd-parity levels is about 300 keV.

Discussion. The SDPF and WDF calculations account for all the known ^{38}Ar states below 5.4-MeV excitation, except the 4710-keV level. The 4710-keV level was given a definite 0^+ assignment by Endt and van der Leun.¹⁸ The evidence for this assignment comes from an $^{36}\text{Ar}(t,p)^{38}\text{Ar}$ angular distribution.⁵⁸ According to one of the authors of that work,⁶⁰ the 0^+ assignment should not be taken as definite. If, in actual fact, there is a $J^\pi=0^+$ level at 4710 keV, it is not predicted by the USD interaction, which places the second 0^+ state at 6182 keV, nor by the WDF interaction, which places the next $2\hbar\omega$ 0^+ state at 7532 keV.

2. ^{38}Cl

The ^{38}Cl results are compared to experiment in Fig. 9.

a. The WDF calculation. The calculation in a $(d_{3/2}f_{7/2})^6$ model space indicates that the $3\hbar\omega$ odd-parity states commence at ~ 2.8 MeV with the 1^- , 2^- , and 4^- states marked by asterisks in Fig. 9. The odd-parity states below these are $> 80\%$ $1\hbar\omega$. The even-parity states shown are all predominantly $2\hbar\omega$ with $4\hbar\omega$ commencing at ~ 4.4 MeV.

b. The SDPF calculation. We discuss two cases.

Odd parity. The odd-parity calculation was done in the full $(sd)^{21}(fp)^1$ space. The rather good agreement for the four lowest levels was expected because of the well-known success of the Pandya⁶¹ transformation between ^{40}K and ^{38}Cl and because our 2BME's were forced to fit the ^{40}K particle-hole spectrum (^{40}Ca , $T=1$ spectrum). In Fig. 9 all the experimental levels with J enclosed in parentheses have definite parity, but a range of J values are allowed. We have chosen the correspondence indicated to give best agreement to the calculation for levels below 2.8-MeV excitation. For the odd-parity levels between 1- and 2-MeV

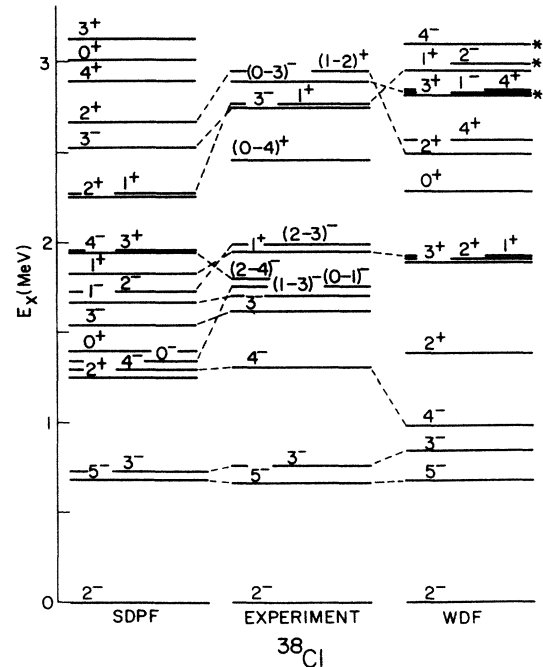


FIG. 9. Comparison of the calculated and experimental level schemes of ^{38}Cl . The experimental data are from Ref. 18. All known states below 3 MeV are shown. Predominantly $3\hbar\omega$ states in the WDF calculation are labeled by asterisks.

excitation, in fact, the correspondence shown is the only one consistent with the experimental ranges in J . Note that the 0^- , 1^- , 2^- , and 3^- states in the 1–2 MeV range do not appear in the WDF spectrum; they are predominantly $\pi d_{3/2} \nu p_{3/2}$. With the identifications indicated, the average rms deviation for the nine odd-parity excited levels is 175 keV.

Even parity. The even-parity spectra was calculated with the SDPF interaction and with two nucleons in the pf shell, i.e., a $2\hbar\omega$ model space. (Of course, $0\hbar\omega$ is not allowed in this case because $N > 20$.) For the calculation of even-parity states truncation of the subshell occupancies was necessary (see Table X). A number of different truncations, displayed in Table XI, were used in an attempt to understand its effect. We return to this subject when the Gamow-Teller decays are discussed. The excitation energies of Fig. 9 correspond to the range of partitions $[10-12, \leq 8, \leq 4; 0 \leq 2, 0, 0, \leq 2, 0]$, where a \leq sign means the subshell occupancy was not restricted. This

TABLE XI. Truncation schemes for calculation of the $^{38}\text{Cl} (sd)^{20}(fp)^2 1^+$ wave functions.

No.	Partitions [$n(d_{5/2}), n(d_{3/2}), n(s_{1/2}); n(f_{7/2}), n(f_{5/2}), n(p_{3/2}), n(p_{1/2})$]	Dimension (no. of J states)
1	[12, $\leq 8, \leq 4; \leq 2, \leq 2, \leq 2$]	465
2	[10–12, $\leq 8, \leq 4; \leq 2, 0, \leq 2, 0$] ^a	1503
3	[$\leq 12, \leq 8, \leq 4; \leq 2, 0, \leq 2, 0$]	2019
4	[11–12, $\leq 8, \leq 4; \leq 2, 0-1, \leq 2, 0-1$]	2066
5	[10–12, $\leq 8, \leq 4; \leq 2, 0-1, \leq 2, 0-1$]; $S \leq 2$	1907

^aThe results of Fig. 9.

calculation provides candidates for the two 1^+ states identified in $^{38}\text{S}(\beta^-)^{38}\text{Cl}$ (see Table VII). The wave functions of these two states are rather similar, both being $\sim 50\%$ $[12,5,3;2,0,0,0]$, i.e., excitation of a $2s_{1/2}$ nucleon into the $d_{3/2}$ orbit. There are only two possible experimental candidates for the predicted 0^+ , 2^+ , 3^+ , and 4^+ states. Thus, it is very likely that about seven even-parity states below ~ 3 MeV in ^{38}Cl remain to be detected. Especially noteworthy is the prediction of a 2^+ state a 1251 keV. Perhaps one of the known levels between 1 and 2 MeV is a doublet. The $^{36}\text{S}(t,n)$ or $^{36}\text{S}(\alpha,d)$ reactions might be useful in the study of these even-parity states.

As an aid to the search for the 2_1^+ state, its electromagnetic decay modes were calculated. We use truncation no. 5 of Table XI—giving a J dimension of 2754—to calculate an excitation energy of 1377 keV and $B(E1)$ values for decay to the 2_1^- and 3_1^- states of 0.96×10^{-4} and $0.37 \times 10^{-5} e^2 \text{fm}^2$, respectively. The $M2$ rates are found to be negligible. These $B(E1)$ values give branching ratios of 99.5% and 0.5% to the 2^- and 3^- states, respectively, and a total lifetime of 2.5 ps.

3. ^{37}Cl

Comparison of our calculated spectra with experiment is shown in Fig. 10. Note that the levels in this figure carry their $2J$ values.

a. The WDF calculation. The results of a calculation in the $(d_{3/2}f_{7/2})^5$ model space using the WDF interaction is shown to the right in Fig. 10. The even-parity states from this calculation are labeled by the intensity of $0\hbar\omega$, $2\hbar\omega$, and $4\hbar\omega$ in the wave function. We see that the WDF interaction predicts five $2\hbar\omega$ states below 5-MeV excitation. The odd-parity states predicted by the WDF interaction for $E_x < 5$ MeV are all $> 83\%$ $1\hbar\omega$. The $3\hbar\omega$ states are predicted to start at ~ 5.2 -MeV excitation with a $\frac{7}{2}^-$ state.

b. The SDPF calculation. We discuss two cases.

Even parity. Experimentally, there are seven definite, two probable, and four possible even-parity levels up to and including the $\frac{7}{2}^+$ state at 4904 keV. The USD and WDF interactions can jointly account for the seven definite even-parity levels and one probable even-parity level.

Odd parity. On the basis of the WDF calculation we expect that the odd-parity states below 5-MeV excitation should all be accounted for by a SDPF $1\hbar\omega$ calculation. The calculations whose results are shown in Fig. 10 do provide possible candidates for all known odd-parity levels up to 5-MeV excitation. There is one missing experimental $\frac{1}{2}^-$ state. (It is possible that the 4269-keV level has $J^\pi = \frac{1}{2}^-$ rather than $\frac{1}{2}^+$.) The 3627-keV level has been given a $J^\pi = \frac{3}{2}^{(+)}$ assignment.¹⁸ We find better accord with the calculations if it has $J^\pi = \frac{3}{2}^-$ rather than $\frac{3}{2}^+$; otherwise, there is a poorly accounted for calculated $\frac{3}{2}^-$ state at 3.5 MeV and an extra $\frac{3}{2}^+$ state (the 3627-keV level) which the calculation cannot easily accommodate. Only one definite $\frac{9}{2}^-$ state is known experimentally. The known properties (from experiment) of either the 4921- or 4932-keV level would be consistent with a $\frac{9}{2}^-$ assignment and thus both are candidates for $\frac{9}{2}^-$.

c. Discussion. The worst defect in our calculations so

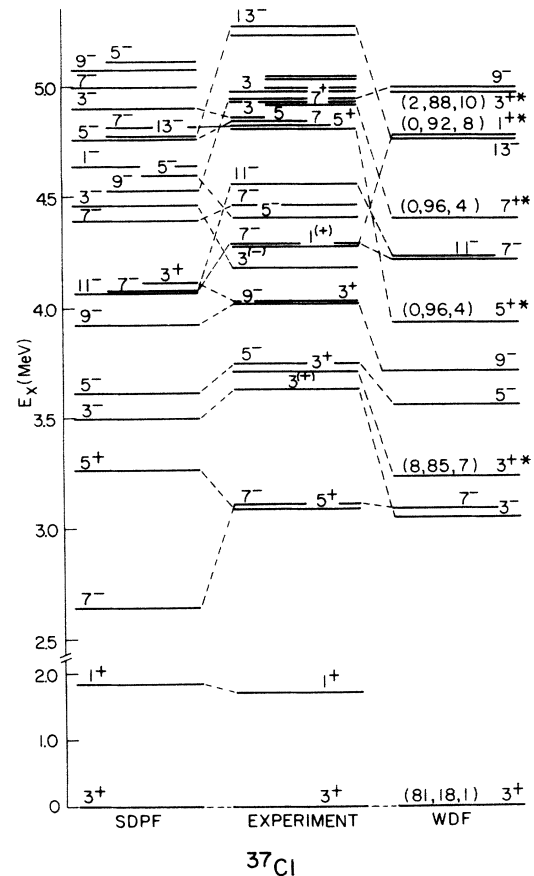


FIG. 10. Comparison of the calculated and experimental level schemes of ^{37}Cl . The levels are labeled with $2J^\pi$. Uncertain parity assignments are in parentheses. The experimental results are mainly from the recent (p,γ) study of Nooren *et al.* (Ref. 23) with supplemental information from Endt and van der Leun (Ref. 18). All definitely known states up to the $\frac{13}{2}^-$ 5271-keV level are shown. The percentages of $0\hbar\omega$, $2\hbar\omega$, and $4\hbar\omega$ in the $\pi = +$ WDF wave functions are given in parentheses, and predominantly $2\hbar\omega$ states are labeled by asterisks.

far encountered is in the excitation energies of the higher spin $(\frac{7}{2} - \frac{13}{2})$ odd-parity levels. The calculated energies are, on the average, about 450 keV too low. On the other hand, the next higher yrast state is predicted to be a $\frac{15}{2}^-$ level at 7648 keV; some 630 keV above the $(\frac{15}{2}^-)$ 7020-keV level¹⁶² to which it probably corresponds. On reflection, there is no reason to expect E_x for the $\frac{15}{2}^-$ state to also be calculated too low since $\frac{13}{2}^-$ is the largest spin one can obtain from $(d_{3/2})^{-4}f_{7/2}$ with the result that different 2BME's and SPE's become dominant for $J^\pi > \frac{13}{2}^-$. In spite of the poor agreement for $J \geq \frac{7}{2}$, the average rms deviation for the 14 odd-parity levels for which a correspondence is indicated in Fig. 10 is about 270 keV, better than for ^{38}Ar .

4. ^{35}S

The comparison to experiment is shown in Fig. 11. The levels are labeled with their $2J$ values. Experimental

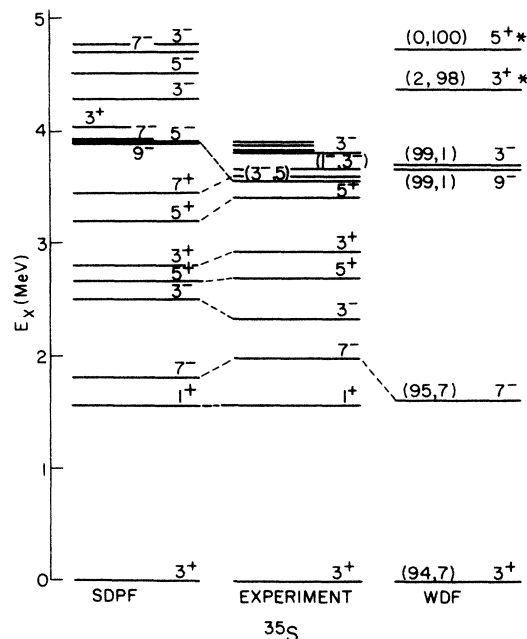


FIG. 11. Comparison of the calculated and experimental level schemes of ^{35}S . The experimental data are mainly from Ref. 35. The levels are labeled with $2J^\pi$. All experimental levels up to 4 MeV are shown. The percentages of $0\hbar\omega$ and $2\hbar\omega$ and of $1\hbar\omega$ and $3\hbar\omega$ in the $\pi=+$ and $\pi=-$ WDF wave functions, respectively, are given in parentheses. Predominantly $2\hbar\omega$ states are labeled by asterisks. For the SDFP calculations all predicted levels up to 5 MeV are shown.

spin-parity assignments are taken from the recent $^{34}\text{S}(n,\gamma)^{35}\text{S}$ study of Raman *et al.*³⁵ and from Endt and van der Leun.¹⁸ Some spin-parity assignments are given in addition to those from Ref. 35. The present β^- decay results yield a definite $\frac{3}{2}^+$ assignment to the 2938-keV level. The γ decays into and out of the 3558-keV level in the (n,γ) reaction strongly suggest $\frac{3}{2}^-$ or $\frac{5}{2}^-$; otherwise, at least one γ transition would be $M2$ or even more unfavored. A probable $l_n=1$ angular distribution from the $^{34}\text{S}(d,p)^{35}\text{S}$ reaction was observed to the 3675-keV level,⁶³ indicating a preference for $J^\pi=\frac{1}{2}^-$ or $\frac{3}{2}^-$.

a. *The WDF calculations.* For ^{35}S the WDF interaction (right-hand side of Fig. 11) predicts the beginning of appreciable $2\hbar\omega$ admixtures in the even-parity states and $3\hbar\omega$ admixtures in the odd-parity states at ~ 4.4 - and 5.5-MeV excitation, respectively. Because ^{35}S is at the lower limit in A of the range of applicability of a $d_{3/2}f_{7/2}$ model, we have also estimated the effects of $2\hbar\omega$ and $3\hbar\omega$ admixtures using the van der Poel interaction,²³ which uses a $s_{1/2}d_{3/2}f_{7/2}p_{3/2}$ model space. With this interaction we find appreciable $2\hbar\omega$ and $3\hbar\omega$ admixtures commencing at ~ 3.8 and 7.2 MeV, respectively. We conclude that levels up to ~ 3.8 MeV are most likely predominantly $0\hbar\omega$ or $1\hbar\omega$.

b. *The SDFP calculation.* We discuss two cases.

Even parity. The even-parity spectrum is just that of the USD. The agreement is quite impressive. The most likely candidate for the unidentified $\frac{7}{2}^+$ state is the

3597-keV level, which decays 100% to the $\frac{3}{2}^+$ ground state with limits on other branches of $<5\%$ each.¹⁸ We have calculated the electromagnetic decays of the $\frac{7}{2}^+$ state of $(sd)^{19}$ in order to check whether or not our SDFP predictions are consistent with the decay of the 3597-keV level. Using extra effective charges of 0.35 for both neutrons and protons for $E2$ transitions and the free-nucleon g factors for $M1$ transitions, we find transition strengths in Weisskopf units (W.u.) of 3.55 and 0.043 for the $\frac{7}{2}^+ \rightarrow \frac{3}{2}^+$ $E2$ and $\frac{7}{2}^+ \rightarrow \frac{5}{2}^+$ $M1$ transitions, respectively. The $\frac{7}{2}^+ \rightarrow \frac{7}{2}^-$ $E1$ transition strength is found to be 7.8×10^{-5} W.u. All other possible decay modes are negligible. The branching ratios are then 93%, 5%, and 2% to $\frac{3}{2}^+$, $\frac{5}{2}^+$, and $\frac{7}{2}^-$, respectively. Thus, we conclude that the 3597-keV level is indeed a good candidate for the lowest $\frac{7}{2}^+$ state.

Odd parity. The SDFP $1\hbar\omega$ calculation for ^{35}S has quite large matrix dimensions (see Table X), so some truncation is necessary. In the calculation of the $1\hbar\omega$ spectrum we used the subshell restrictions $[10-12, \leq 8, \leq 4; 0-1, 0, 0-1, 0]$. This gives $(2J:\text{dimension}) = (1:1052), (3:1893), (5:2358), (7:2431), \text{ and } (9:2147)$, which is manageable. The $\frac{7}{2}^-$ and $\frac{3}{2}^-$ predictions are in good accord with experiment. The lowest-lying experimental candidate for the $\frac{5}{2}^-$ state is that at 3558 keV compared to a prediction of 3916 keV. The $\frac{9}{2}^-$ state is as yet unidentified. The two lowest-lying possibilities are the 3818- and 4022-keV levels, both of which have $\sim 100\%$ decays to the $\frac{7}{2}^-$ 1991-keV level. Either would be in good agreement with the predicted excitation energy of 3910 keV for $\frac{9}{2}^-$.

5. Ground-state binding energies

Calculated and experimental ground-state binding energies are compared in Table XII. For the four nuclei at the top of the table the states are predominantly $(sd)^n$ and the differences between the calculated and experimental binding energies of the ground states are given.^{59,64} For the lower three nuclei, the comparison is of a $(n+1)\hbar\omega$, $T+1$ state (the analog of the β^- emitter) relative to the $n\hbar\omega$, T ground state. It is seen that the tendency—noted for ^{37}Cl —for the SDFP interaction to give $1\hbar\omega$ states too low is seen here as well.

C. Gamow-Teller transitions

Allowed rates were calculated for the beta decays of ^{35}P , ^{37}S , ^{38}S , and ^{38}Cl . The calculations were carried out both with the free-nucleon Gamow-Teller operator and with an effective Gamow-Teller operator. The parameters of the effective operator were taken to be the “final fit” values given in Table B of Brown and Wildenthal,⁴ but with $\delta_s(s-s)$ set equal to $\delta_s(d-d)$ since the difference is essentially negligible and the calculation is easier with them equal. These parameters are $\delta_s(d-d) = -0.248(11)$, $\delta_l(d-d) = 0.004(3)$, and $\delta_p(d-d) = \delta_p(s-d) = 0.017(8)$. These empirical parameters result from a least squares fit to Gamow-Teller (GT) transitions between levels in $A=17-39$ nuclei which are well described in the $(2s,1d)$

TABLE XII. Comparison of calculated and experimental binding energies.

Nucleus	$J^\pi; T_Z$	Excitation energy in $T_Z - 1$ nucleus (keV)		$\Delta(\text{expt.} - \text{calc.})$ (keV)
		Expt. ^a	SDPF	
³⁵ S	$\frac{3}{2}^+; \frac{3}{2}$			-190
³⁵ P	$\frac{1}{2}^+; \frac{5}{2}$			168
³⁷ Cl	$\frac{3}{2}^+; \frac{3}{2}$			217
³⁸ Ar	0 ⁺ ; 1			-1
³⁷ S	$\frac{7}{2}^-; \frac{5}{2}$	10 224	9890	334
³⁸ Cl	2 ⁻ ; 2	10 626	10 178	448
³⁸ S	0 ⁺ ; 3	8216	7791	425

^aReference 18.

configurational space. They result in a quenching of 50–55% in the upper part of the (2s, 1d) shell. These *sd*-shell parameters are not necessarily appropriate for the *fp* shell. However, quenching present in the ⁴¹Sc(β^+)⁴¹Ca GT mirror decay is comparable to that in GT transitions in the upper part of the *sd* shell.⁶ Also, Towner and Khanna⁶—whose first principles calculation explains the *sd* shell GT parameters so well—predict similar results in $A = 41$. Thus, we feel justified in using the same effective operator quenching throughout the SDPF region. Note that the departures of the effective GT operator from the free nucleon operator presumably include the results of

n -particle, n -hole admixtures, and, in fact, because of tensor correlations one must include excitations up to $n \sim 10$ (Ref. 6).

The calculations for ³⁵P, ³⁷S, and ³⁸Cl decay were done in the SDPF space with the *pf* occupancy restricted to the lowest allowed by the parities of the states involved. For ³⁸S(0⁺) \rightarrow ³⁸Cl(1⁺) the dimension of the (*sd*)²⁰(*fp*)² matrix of 1⁺ states was too large as already discussed and some truncation was necessary. The calculation was done approximately by calculating in the truncated basis nos. 1–4 of Table XI. For each of these calculations the one-body-density (OBD) overlap with the ³⁸S 0⁺ state (calcu-

TABLE XIII. Comparison of experimental and calculated Gamow-Teller rates for the decay of ³⁵P, ³⁷Cl, ³⁸S, and ³⁸Cl.

Decaying body	$J_i^\pi; T_i$	E_f (keV)	J_f^π	$10^3 B_0(\text{expt.})$	$10^3 B_0(\text{calc.})$	
					Effective	Free
³⁵ P	$\frac{1}{2}^+; \frac{5}{2}$	0	$\frac{3}{2}^+$		0.42	0.03
		1572	$\frac{1}{2}^+$	462(7)	518	878
		2938	$\frac{3}{2}^+$	67(4)	91	173
³⁷ S	$\frac{7}{2}^-; \frac{5}{2}$	3104	$\frac{7}{2}^-$	254(2)	232	377
		3741	$\frac{5}{2}^-$	5(1)	17	33
		4010	$\frac{9}{2}^-$	4(1)	10	17
		4273	$\frac{7}{2}^-$	11(1)	85	145
		4396	$\frac{5}{2}^{(-)}$	2(1)	9	16
		4460	$\frac{7}{2}^-$	< 14	21	30
		4811	$\frac{7}{2}^-$		11	20
		4838	$\frac{5}{2}^-$		5	10
³⁸ S	0 ⁺ ; 3	1942	1 ⁺	66(4)	9(27) ^a	20(46) ^a
		2751	1 ⁺	440(90)	234(219) ^a	481(454) ^a
³⁸ Cl	2 ⁻ ; 2	3810	3 ⁻	74(2)	102	182
		4877	3 ⁻		32	50

^aThe first number is the “hybrid” calculation. The second (in parentheses) is from truncation no. 5 of Table XI.

lated in the full SDPF space) was formed. These were then combined so as to form a “hybrid” full SDPF OBD. Tests of similar cases but with smaller dimensions showed this to be a very good approximation to the full calculation. As a final check the calculation was done in the “broken pair” truncation, $S \leq 2$ —the last listing in Table XI. Results are collected in Table XIII. We consider the general agreement for the four decaying bodies as quite good. There is an obvious and gratifying preference for calculations done with the effective operator. None of the transitions are especially strong; however, the stronger transitions are calculated as such and we do not expect as good agreement for the weaker transitions (say $10^3 B_0 < 100$). The worst discrepancy is for $^{38}\text{S}(\beta^-)^{38}\text{Cl}$, the only case involving two particles in the (fp) shell. As far as we know, this is the first calculation which gives a reasonable explanation of any of the allowed decays of ^{37}S , ^{38}S , or ^{38}Cl . For ^{35}P decay, the fp shell is not involved and the calculated results are those of the USD interaction as reported by Brown and Wildenthal.⁴

D. Unique first-forbidden transitions

In this subsection we consider the unique first-forbidden, i.e., $\Delta J=2$, $\Delta\pi=-$, decays of ^{35}P , ^{37}S , ^{38}S , and ^{38}Cl . These $M2$ -like beta transitions provide a natural test of our interaction since they directly involve the cross-shell part between the (sd) and (pf) shells. In unique first-forbidden beta decay ($n_i l_i j_i$) and ($n_f l_f j_f$) may differ by only one major oscillator quantum ($2n+l-2$). Thus, the SDPF space provides a complete basis for these first-forbidden decays assuming an inert ^{16}O core.

The history of our understanding of unique first-forbidden decays in this mass region is an interesting one. Early attempts to understand them utilized a $d_{3/2}f_{7/2}$

model space and were unsuccessful. Oquidam and Janovici⁶⁵ first showed that unique first-forbidden decays in this region were retarded by a rather constant factor of ~ 5 relative to decay rates obtained from wave functions diagonalized in a $d_{3/2}f_{7/2}$ space. Bertsch and Molinari⁶⁶ then gave some insight into the nature of this retardation in a treatment of ^{17}N , ^{39}Ar , and ^{41}Ca decays. However, ^{39}Ar and ^{41}Ca decays were unfortunate cases to treat as most of the inhibition results from cancellation effects within the $d_{3/2}f_{7/2}$ model space which render the result very sensitive to the interaction.

The inhibition was convincingly and essentially completely explained by the first-order perturbative treatment of Towner *et al.*,¹³ who showed it to be due to general properties of the repulsive particle-hole interaction such that the $\sim 10\%$ of the wave functions not $d_{3/2}f_{7/2}$ in both initial and final states acted coherently in destructive phase to the main $d_{3/2}f_{7/2}$ contribution. Because the effect depends on rather general properties of the interaction which our SDPF interaction should possess, we should expect to obtain similar results and with no surprises. However, there are several reasons to calculate these decays. First, the 1971 calculation of Towner *et al.*¹³ was done perturbatively and has not been checked since with a full diagonalization of the SDPF space. Second, Towner *et al.*¹³ displayed with a schematic model calculation the specific dependence of the hindrance on the nucleon-nucleon potential; thus, a comparison to experiment should help test the cross-shell part of our interaction and any discrepancies with experiment would be especially informative.

Comparison to experiment is made in Table XIV in which we collect the experimental transition rates, B_1 , from the previous tables. Our calculation uses harmonic oscillator radial wave functions with the length parameter $b = (41.467/\hbar\omega)^{1/2}$ fm with $\hbar\omega = 45A^{-1/3} - 25A^{-2/3}$

TABLE XIV. Comparison of experimental and calculated unique first-forbidden rates for the decay of ^{35}P , ^{37}Cl , ^{38}S , and ^{38}Cl .

Decaying body	$J_i^\pi; T_i$	E_f (keV)	J_f^π	$B_1(\text{expt.})$ (fm ²)	$B_1(\text{calc.})$ (fm ²)		
					(a)	(b)	(c)
^{35}P	$\frac{1}{2}^+; \frac{5}{2}$	(3558) ^d	$\frac{5}{2}^-$	$< 2 \times 10^5$	0	0.19	
^{37}S	$\frac{7}{2}^-; \frac{5}{2}$	0	$\frac{3}{2}^+$	1.32(14)	14.08	6.11	
		3708 ^e	$\frac{3}{2}^+$	< 7.3	0	e	
		4016	$\frac{3}{2}^+$	< 23	0	0.009	
^{38}S	$0^+; 3$	0	2^-	2.12(54)	28.93	8.92	
		1981	(2) ⁻	< 6	0	0.036	
^{38}Cl	$2^-; 2$	0	0^+	1.67(4)	11.57	6.08	2.62(2.95) ^f
		3377	0^+	< 0.71	0	0	0.003

^{a-c}See text.

^dThis is a speculation (see Fig. 11).

^eThis level is assumed to be an intruder (see Fig. 10) and the 4016-keV level is assumed to be the second $\frac{3}{2}^+$ state of the SDPF space.

^fThe first number is the “hybrid” calculation. The second (in parentheses) is from truncation no. 4 of Table XVI.

TABLE XV. The $^{38}\text{Cl}(\beta^-)^{38}\text{Ar } 2^- \rightarrow 0^+$ transition rate B_1 (in fm^2) calculated in a $d_{3/2}f_{7/2}$ model space with the indicated $n\hbar\omega$ contributions to the initial (n_i) and final (n_f) state.

n_i	n_f			
	0	0+2	0+2+4	0+2+4+6
1	11.57	6.83 ^a	6.10	6.05
1+3	9.88	7.75	6.93 ^a	6.88
1+3+5	9.56	7.69	6.96	6.88 ^a

^aThese values correspond to the smallest final model space necessary to connect to all components of the initial state.

MeV. We first consider the calculation of B_1 given in column (a). This is the value for the $d_{3/2}f_{7/2}$, $2\hbar\omega \rightarrow 1\hbar\omega$, or $1\hbar\omega \rightarrow 0\hbar\omega$ model. $^{35}\text{P}(\beta^-)^{35}\text{S}$ lies outside this model space, the other three decays are all extremely simple with only one nonzero B_1 and that easily related to the $d_{3/2} \leftrightarrow f_{7/2}$ single-particle B_1 value.¹³ The inhibition for this calculation, i.e., $B_1(df)/B_1(\text{expt})$ is a factor of 10.7, 13.6, and 6.9 for ^{37}S , ^{38}S , and ^{38}Cl , respectively, exhibiting the hindrance we have discussed. To explain this hindrance it is necessary to utilize the full SDPF space in the $1\hbar\omega$ or $2\hbar\omega$ initial ($T_>$) state and include $2\hbar\omega$ or $3\hbar\omega$ excitations in the final ($T_<$) state which is predominantly $0\hbar\omega$ or $1\hbar\omega$. This was transparently explained by the treatment of Towner *et al.*¹³ The effects of the full SDPF space in the initial state are the largest but inclusion of correlations in the final state is also necessary in order to explain the hindrance. This latter point is discussed further below. The use of a full SDPF space for the initial state is easily accomplished. It is just what we have done to obtain the energy level spectra of Figs. 8–11. If we use these wave functions to calculate the B_1 , we obtain the results of column (b). The hindrance has been cut to 4.6, 4.2, and 3.6 for ^{37}S , ^{38}S , and ^{38}Cl and now we have finite, albeit small, values of B_1 for decays to excited states and for ^{35}P decay to the unknown $\frac{5}{2}^-$ state.

How does this result compare to the perturbative treatment of Towner *et al.*?¹³ In our calculation, the inclusion of all SDPF particle-hole terms cuts the transition strength B_1 for ^{37}S , ^{38}S , and ^{38}Cl by factors of 0.43, 0.31, and 0.53, respectively. Towner *et al.*¹³ obtained factors of 0.36, 0.30, and 0.41, respectively. The agreement is impressive.⁶⁷

We now consider ground-state correlations, by which we mean admixtures of higher $n\hbar\omega$ terms to the initial and final states. We first illustrate the effect by calculat-

ing the $^{38}\text{Cl}(\beta^-)^{38}\text{Ar } 2^- \rightarrow 0^+$ B_1 in a $d_{3/2}f_{7/2}$ model space with all possible permutations of restrictions on the np - nh contributions to initial and final states. The results are shown in Table XV. This exercise illustrates that a good approximation to the full $(d_{3/2}f_{7/2})^6$ result, i.e., $\leq 5\hbar\omega \rightarrow \leq 6\hbar\omega$, is obtained if the final state wave function contains all $n\hbar\omega$ terms which can connect to the initial state. This can be understood by noting (a) all $(n+1)\hbar\omega \rightarrow (n+2)\hbar\omega$ terms have the same phase which is opposite to all $(n+1)\hbar\omega \rightarrow n\hbar\omega$ terms, and (b) the reduction due to normalization as the number of $n\hbar\omega$ terms increases is compensated for by the additional in-phase contribution. Thus, in calculations of the B_1 it is reasonable to confine our calculations to the lowest $(n+1)\hbar\omega$ allowed for the initial state and $n\hbar\omega + (n+2)\hbar\omega$ for the final state. This result was explained by Towner *et al.*¹³ Expansion of the model space to SDPF will not affect the general principle, but will increase the magnitude of the effect of adding $(n+2)\hbar\omega$ terms in the final state.

Unfortunately, inclusion of $2\hbar\omega$ states in a full SDPF calculation is beyond our computational capabilities and only for the $^{38}\text{Ar } 0^+$ states can we come close enough to a full SDPF space to perform a meaningful calculation. For $^{38}\text{Cl}(\beta^-)^{38}\text{Ar}$ the calculation was done with a full SDPF $1\hbar\omega$ wave function for ^{38}Cl , while for the $^{38}\text{Ar } 0^+$ states we considered several truncation schemes much as for the $^{38}\text{Cl } 1^+$ states described in the preceding subsection. These are listed in Table XVI. The final “hybrid” result was obtained by combining OBD’s for the first three truncations in the table. Finally, close to the fullest possible calculation of the $^{38}\text{Ar } 0^+$ wave functions was performed by truncating with a specific list of partitions as summarized in Table XVI. As is seen in Table XIV, the final results for ^{38}Cl decay are in reasonable accord with experiment but fall short of explaining the inhibition by $\sim 60\%$. This discrepancy is not disturbing for two reasons. First, as discussed in Sec. V A, we have reasons to view the $(0+2)\hbar\omega$ calculation of ^{38}Ar with some caution. Second, in analogy with Gamow-Teller decay, it would appear likely that there is further quenching beyond $2\hbar\omega$ correlations and possibly also from Δ -isobar and mesonic effects.⁶⁸

The results presented for ^{38}Cl decay would appear to constitute a sufficient test of the perturbative treatment of Towner *et al.*,¹³ who obtained good agreement for the $^{38}\text{S}(\beta^-)$ and $^{37}\text{S}(\beta^-)$ ground-state decays as well as for this decay. The calculation of the $(0+2)\hbar\omega$ $^{38}\text{Ar } 0^+$ wave

TABLE XVI. Truncation schemes for calculation of the $^{38}\text{Ar}(0+2)\hbar\omega$ 0^+ wave functions.

No.	Partitions	Dimensions
	$[n(d_{5/2}), n(d_{3/2}), n(s_{1/2}); n(f_{7/2}), n(f_{5/2}), n(p_{3/2}), n(p_{1/2})]$	(no. of J states)
1	$[10-12, \leq 8, \leq 4; \leq 2, 0, \leq 2, 0]$	1107
2	$[10-12, \leq 8, 4; \leq 2, \leq 2, \leq 2, \leq 2]$	1155
3	$[12, \leq 8, \leq 4; \leq 2, \leq 2, \leq 2, \leq 2]$	412
4	the 51 (of 156 total) most important partitions as estimated from the above results (m -scheme dimension = 78 367)	1699

TABLE XVII. Comparison of the one-body-density amplitudes for the unique first-forbidden $^{38}\text{Cl}(\beta^-)^{38}\text{Ar}$ g.s. decay for two model spaces.

j_f	j_i	$N_i\text{OBD}(0)$	$\text{OBD}(0+2)$
$d_{5/2}$	$f_{7/2}$	+ 0.086 25	+ 0.086 42
$d_{5/2}$	$f_{5/2}$	- 0.043 33	- 0.043 36
$d_{5/2}$	$p_{3/2}$	+ 0.007 62	+ 0.007 66
$d_{5/2}$	$p_{1/2}$	- 0.015 75	- 0.015 76
$d_{3/2}$	$f_{7/2}$	- 0.772 70	- 0.772 70
$d_{3/2}$	$f_{5/2}$	+ 0.016 77	+ 0.016 78
$d_{3/2}$	$p_{3/2}$	- 0.087 92	- 0.087 72
$d_{3/2}$	$p_{1/2}$	+ 0.010 49	+ 0.010 49
$s_{1/2}$	$f_{5/2}$	- 0.015 28	- 0.015 24
$s_{1/2}$	$p_{3/2}$	+ 0.170 40	+ 0.170 01

function provides an additional confirmation of the perturbative approach to the calculation of the $^{38}\text{Cl}(\beta^-)^{38}\text{Ar}$ g.s. transition. For perturbation theory to be valid it is necessary, to a sufficient approximation, that the deviations from the $d_{3/2}f_{7/2}$ result due to corrections to the initial and final states can be treated independently. One way to satisfy this condition is for the $0\hbar\omega$ part of the 0^+ g.s. wave function to be approximately the same for the $0\hbar\omega$ and $(0+2)\hbar\omega$ calculations. That they are the same to an extraordinary accuracy is shown in Table XVII, where we compare the OBD's for the $0\hbar\omega$ and $(0+2)\hbar\omega$ calculations. In both cases the OBD is taken for a $(JT)=(21)$ tensor between the full SDPF $1\hbar\omega$ 2^- ^{38}Cl initial state and the 0_1^+ final state. The normalization factor N_i is the amplitude of $0\hbar\omega$ wave function in the mixed $(0+2)\hbar\omega$ wave function. In this case it is 0.8907. The $(0+2)\hbar\omega$ calculation used here is no. 1 of Table XVI. It is clear that the $0\hbar\omega$ part of the wave function is essentially unchanged by the mixing in of the 20.7% $2\hbar\omega$ component.

It is interesting to note that the converse of this last statement is not true. If a calculation is made of ^{38}Ar 0^+ states in a $2\hbar\omega$ space $(sd)^{20}(fp)^2$ and we inquire as to the overlap of the $2\hbar\omega$ part of our previously calculated $(0+2)\hbar\omega$ ground state with this spectrum of $2\hbar\omega$ states, we find only a small overlap with the lowest $2\hbar\omega$ state. Only 60% of the complete overlap is found in the first 35 MeV of excitation and this is spread with $\sim 25\%$ clustered near 16 MeV and $\sim 20\%$ in the second $2\hbar\omega$ state at ~ 7 -MeV excitation (all excitations are relative to assuming the $2\hbar\omega$ states commence at 3.38 MeV). (It is interesting that the spectrum of unique first-forbidden strength for the ^{38}Cl ground state has a roughly similar shape.) We conclude that the composition of the $2\hbar\omega$ part of the $(0+2)\hbar\omega$ 0^+ ground state of ^{38}Ar is quite complex and is not amenable to a simple explanation.

VI. SUMMARY

The β decays of ^{35}P , ^{37}S , ^{38}S , and ^{38}Cl were investigated by γ -ray spectroscopy. These are all the nuclei which can be most easily formed by bombardment of ^{36}S with light ($A \leq 4$) projectiles. Two new decays were observed: $^{35}\text{P}(\beta^-)^{35}\text{S}(2938\text{-keV level})$ and $^{38}\text{S}(\beta^-)^{38}\text{Cl}(1692\text{-keV level})$. More accurate E_γ and I_γ values were obtained for

many transitions and more stringent limits were placed on most energetically accessible but unobserved transitions.

From comparison of the experimental Gamow-Teller results with the known and predicted energy levels of the daughter nuclei, it is concluded that, with one exception, all the energetically allowed GT decays that are measurable with present-day techniques have been found. The one exception is ^{35}P decay to the ^{35}S $\frac{3}{2}^+$ ground state. In ^{38}Cl decay the 3_2^- state at 4877-keV excitation is energetically accessible ($Q_0=4917$ keV) and in ^{37}S decay we predict (Fig. 10) that $\frac{7}{2}^-$ and $\frac{5}{2}^-$ lie at 4811 and 4838 keV, respectively, and thus are accessible ($Q_0=4865$ keV), but in these cases the phase space available is so small as to effectively prohibit observation of the decays which are predicted to have relatively small GT rates.

From a perusal of the experimental data and the shell-model predictions, one concludes that all unique first-forbidden decays which are expected to be observable have also been seen. There are several unobserved but energetically accessible decays (see Table XIV), but all are predicted to have such small transition strengths as to be essentially unobservable.

We have described in some detail the construction of a shell-model interaction appropriate for mixed (sd) and (pf) configurations. The results obtained for binding energies are about as good as expected for a first try. The calculation of the Gamow-Teller rates gives the first reasonable explanation of these decays, while the calculation of the unique first-forbidden rates gave added credibility to the perturbative results of Towner *et al.*¹³

As already noted, the GT predictions for the effective operator agree better with experiment than those for the free-nucleon operator. Thus we can say that quenching for the allowed transitions is consistent with the systematics for the sd shell. What can we say about quenching in unique, first-forbidden decays? In the one case we were able to calculate there appears to be a need for some quenching beyond that generated by the repulsive $T=1$ particle-hole interaction and incorporated in the calculation. However, there is such a severe inhibition from this latter source that we consider this evidence to be only suggestive.

A shell-model calculation for neutron rich $A=35-41$ nuclei was recently made by Woods,⁶⁹ who constructed interactions in the $d_{5/2}d_{3/2}s_{1/2}f_{7/2}p_{3/2}$ model space. One of these interactions was also based on the Wildenthal USD interaction. There is not too much overlap between Woods's results and ours. She considered spectroscopic factors and electromagnetic decays but not non-normal parity spectra or beta decay. The only overlap is in the $1\hbar\omega$ spectrum of ^{38}Cl . (She also presented the USD ^{37}Cl $0\hbar\omega$ spectrum, as did we.)

We conclude with two remarks concerning future efforts. First, the calculation in a full SDPF space demands a large scale computer program. Our resources were only adequate for a part of the study we would have liked to pursue; for this, considerably more computer memory is needed. When our computer resources were not adequate for a complete SDPF calculation, we resorted to truncation of the model space. An obvious criticism of our study is the largely unknown effects of such truncation.

There is an obvious need for exploration of the effects of different schemes for truncation of this model space.

Our second remark concerns future improvements in the interaction. We feel we have gone just about as far as one can with *ad hoc* changes in the 2BME's. We suggest that the natural next step is a least-squares adjustment of a rather general potential to selected binding energies, such as was mentioned in the Introduction, was under-way⁸⁻¹⁰ for the similar ¹⁶O region.

ACKNOWLEDGMENTS

Throughout this study D. J. Millener provided a great deal of important assistance and advice, particularly in

the choice of and adjustments to the shell-model interaction SDPF. B. H. Wildenthal kindly provided us with the interaction WDF. Gordon Struble and D. R. Manatt of Lawrence Livermore National Laboratory (LLNL) provided generous assistance to those of us (J.A.B.) and (E.K.W.) utilizing the LLNL Chemistry Division VAX for these calculations. This research was supported by the U.S. Department of Energy, under Contracts No. DE-AC02-76CH00016 with the Associated Universities, Inc. (Brookhaven National Laboratory) No. W-7405-Eng-48 with the University of California (LLNL), and No. DE-AC05-84OR21400 with Martin Marietta Energy Systems, Inc. (Oak Ridge National Laboratory).

- ¹S. Cohen and D. Kurath, Nucl. Phys. **73**, 1 (1965).
²B. M. Freedom and B. H. Wildenthal, Phys. Rev. C **6**, 1633 (1972); W. A. Lanford and B. H. Wildenthal, *ibid.* **7**, 668 (1973); W. Chung, Ph.D. thesis, Michigan State University, 1976.
³B. H. Wildenthal, Prog. Part. Nucl. Phys. **11**, 5 (1984); B. H. Wildenthal, M. S. Curtin, and B. A. Brown, Phys. Rev. C **28**, 1343 (1983).
⁴B. A. Brown and B. H. Wildenthal, At. Data Nucl. Data Tables **33**, 347 (1985).
⁵B. A. Brown and B. H. Wildenthal, Phys. Rev. C **28**, 2397 (1983).
⁶I. S. Towner and F. C. Khanna, Nucl. Phys. **A399**, 334 (1983).
⁷D. J. Millener and D. Kurath, Nucl. Phys. **A255**, 315 (1975).
⁸D. J. Millener, private communication.
⁹P. W. M. Glaudemans, in *International Symposium on Nuclear Shell Models*, edited by M. Vallieres and B. H. Wildenthal (World-Scientific, Singapore, 1985), p. 2.
¹⁰B. A. Brown, private communication.
¹¹J. B. McGrory, Phys. Lett. **33B**, 327 (1970).
¹²J. A. Becker and E. K. Warburton, Phys. Rev. Lett. **26**, 143 (1971).
¹³E. K. Warburton, G. T. Garvey, and I. S. Towner, Ann. Phys. (N.Y.) **57**, 174 (1970); I. S. Towner, E. K. Warburton, and G. T. Garvey, *ibid.* **66**, 674 (1971).
¹⁴E. K. Warburton, J. J. Kolata, J. W. Olness, A. R. Poletti, and Ph. Gorodetzky, At. Data Nucl. Data Tables **14**, 147 (1974).
¹⁵J. C. Hill, Phys. Rev. C **9**, 1453 (1974).
¹⁶J. Libert, G. Klotz, P. Baumann, and G. Walter, Nucl. Phys. **A223**, 620 (1974).
¹⁷S. Raman, W. Ratynski, E. T. Jurney, M. E. Bunker, and J. W. Starner, Phys. Rev. C **30**, 26 (1984).
¹⁸P. M. Endt and C. van der Leun, Nucl. Phys. **A310**, 1 (1978).
¹⁹C. E. Thorn, J. W. Olness, E. K. Warburton, and S. Raman, Phys. Rev. C **30**, 1442 (1984).
²⁰D. E. Alburger, E. K. Warburton, and B. A. Brown, Phys. Rev. C **30**, 1005 (1984).
²¹J. T. Routti and S. G. Prussin, Nucl. Instrum. Methods **72**, 125 (1969).
²²J. W. Olness, E. K. Warburton, D. E. Alburger, C. J. Lister, and D. J. Millener, Nucl. Phys. **A373**, 13 (1982).
²³G. J. L. Nooren and C. van der Leun, Nucl. Phys. **A423**, 197 (1984); G. J. L. Nooren, H. P. L. de Esch, and C. van der Leun, *ibid.* **A423**, 228 (1984).
²⁴R. A. Meyer, private communication of Lawrence Livermore Laboratory Report No. M-100 (Dec. 1, 1978) (unpublished). This report is available from R. A. Meyer.
²⁵E. K. Warburton and D. E. Alburger, Nucl. Instrum. Methods **178**, 443 (1980).
²⁶R. G. Helmer, P. H. H. Van Assche, and C. van der Leun, At. Data Nucl. Data Tables **24**, 39 (1979).
²⁷S. Wirjoamidjojo and B. D. Kern, Phys. Rev. **163**, 1094 (1967).
²⁸A. H. Wapstra and G. Audi, Nucl. Phys. **A432**, 1 (1985).
²⁹D. H. Wilkinson, *Nuclear Physics with Heavy Ions and Mesons*, 1977, Les Houches Lectures, edited by R. Balian, M. Rho and G. Ripka (North-Holland, Amsterdam, 1978), p. 955; Nucl. Phys. **A377**, 474 (1982).
³⁰The factor 6166 is from Ref. 29 and supersedes the constants used in Ref. 13. The definition of the transition strength used in Ref. 13 is different than Eq. (2). The present definition of B_n is made so that $B_0 [=B(GT)]$ conforms to the most common present-day usage. The two definitions are related by $B_n = (g_A/g_V)^2 \langle G_n \rangle^2$, where we use $g_A/g_V = -1.2605$ (Ref. 29).
³¹W. Grimm and W. Herzog, Z. Naturforsch. **26a**, 1933 (1971).
³²K. E. Apt and J. D. Knight, Phys. Rev. C **6**, 842 (1972).
³³D. R. Goosman and D. E. Alburger, Phys. Rev. C **6**, 820 (1972).
³⁴S. Khan, Th. Kihm, K. T. Knöpfle, G. Mairle, V. Bechtold, and L. Friechich, Phys. Lett. **156B**, 155 (1985).
³⁵S. Raman, R. F. Carlton, J. C. Wells, E. T. Jurney, and J. E. Lynn, Phys. Rev. C **32**, 18 (1985).
³⁶The value of 1572.372(100) keV reported in Ref. 35 is based on an energy calibration which utilized obsolete values for the neutron binding energies of ²H and ¹³C. When corrected for the best current neutron binding energies, the result is lowered by 74 eV and is more accurate.
³⁷D. R. Nethaway and A. A. Caretto, Phys. Rev. **109**, 504 (1958).
³⁸G. A. P. Engelbertink and J. W. Olness, Phys. Rev. C **3**, 180 (1971).
³⁹J. Visser and L. Lindner, Radiochim. Acta **17**, 212 (1972).
⁴⁰E. K. Warburton and D. E. Alburger, Phys. Rev. C **23**, 1234 (1981).
⁴¹J. Van Klinken, F. Pleiter, and H. T. Dijkstra, Nucl. Phys. **A112**, 372 (1968).
⁴²A. M. J. Spits and J. A. Akkermans, Nucl. Phys. **A215**, 260 (1973).
⁴³J. P. Schiffer and W. W. True, Rev. Mod. Phys. **48**, 191 (1976).
⁴⁴H. Sagawa, B. A. Brown, and O. Scholten, Phys. Lett. **159B**, 228 (1985).
⁴⁵C. J. Van der Poel, Ph.D. dissertation, Utrecht University, 1982.

- ⁴⁶P. M. Endt, *At. Data Nucl. Data Tables* **19**, 23 (1977).
- ⁴⁷A. G. M. van Hees and P. W. M. Glaudemans, *Z. Phys.* **303**, 267 (1980).
- ⁴⁸J. E. Kooops and P. W. M. Glaudemans, *Z. Phys. A* **280**, 181 (1977).
- ⁴⁹A. Hosaka, K. I. Kubo, and H. Toki, *Nucl. Phys.* **A444**, 76 (1985).
- ⁵⁰B. C. Metsch and P. W. M. Glaudemans, *Z. Phys.* **307**, 251 (1982); R. B. M. Mooy and P. W. M. Glaudemans, *ibid.* **312**, 59 (1983).
- ⁵¹Although well known to shell-model practitioners, this difficulty with mixed $n\hbar\omega$, $(n+2)\hbar\omega$, $(n+4)\hbar\omega$, . . . configurations is not well documented. One good early reference is that of Ellis and Zamick (Ref. 52).
- ⁵²P. J. Ellis and L. Zamick, *Ann. Phys. (N.Y.)* **55**, 61 (1969).
- ⁵³M. W. Kirson, in *International Symposium on Nuclear Shell Models*, Ref. 9, p. 290.
- ⁵⁴B. H. Wildenthal, private communication.
- ⁵⁵B. A. Brown, A. Etchegoyen, W. D. M. Rae, and N. S. Godwin, OXBASH, 1984 (unpublished).
- ⁵⁶D. H. Gloeckner and R. D. Lawson, *Phys. Lett.* **53B**, 313 (1974).
- ⁵⁷P. Betz, H. Ropke, F. Glatz, G. Hammel, V. Glattes, and W. Brendler, *Z. Phys. A* **271**, 195 (1974).
- ⁵⁸E. R. Flynn, O. Hansen, R. F. Casten, J. D. Garrett, and F. Ajzenberg-Selove, *Nucl. Phys.* **A246**, 117 (1975).
- ⁵⁹A comprehensive report of results of the USD interaction has not as yet been published. However, a summary of binding energies for $A = 17-39$ has been privately circulated by B. H. Wildenthal.
- ⁶⁰O. Hansen, private communication.
- ⁶¹S. P. Pandya, *Phys. Rev.* **103**, 956 (1956).
- ⁶²P. Baumann, A.-M. Bergdolt, G. Bergdolt, A. Huck, G. Klotz, G. Walter, H. V. Klapdor, H. Fromm, and H. Willmes, *Phys. Rev. C* **18**, 2110 (1978).
- ⁶³J. G. van der Baan and H. G. Leighton, *Nucl. Phys.* **A170**, 607 (1971).
- ⁶⁴A description of the method used to calculate the Coulomb contribution to the experimental binding energies is given in Ref. 2.
- ⁶⁵B. Oquidam and B. Jancovici, *Nuovo Cimento* **11**, 578 (1959).
- ⁶⁶G. Bertsch and A. Molinari, *Nucl. Phys.* **A148**, 87 (1970).
- ⁶⁷However, the calculations are not exactly analogous. We have included all SDPF terms in both the initial and final states, whereas the results quoted from Ref. 13 correspond to a $d_{3/2}f_{7/2}$ space for the final state. The difference is insignificant because the extra terms added in our full SDPF calculation involve transitions between small components.
- ⁶⁸P. Blunden, B. Castel, and H. Toki, *Nucl. Phys.* **A440**, 647 (1985).
- ⁶⁹C. L. Woods, *Nucl. Phys.* **A451**, 413 (1986).